

# The complex influence of ENSO on droughts in Ecuador

S. M. Vicente-Serrano<sup>1</sup> · E. Aguilar<sup>2</sup> · R. Martínez<sup>3</sup> · N. Martín-Hernández<sup>1</sup> ·  
C. Azorin-Molina<sup>1</sup> · A. Sanchez-Lorenzo<sup>1</sup> · A. El Kenawy<sup>4,5</sup> · M. Tomás-Burguera<sup>6</sup> ·  
E. Moran-Tejeda<sup>1</sup> · J. I. López-Moreno<sup>1</sup> · J. Revuelto<sup>1</sup> · S. Beguería<sup>6</sup> · J. J. Nieto<sup>3</sup> ·  
A. Drumond<sup>7</sup> · L. Gimeno<sup>7</sup> · R. Nieto<sup>7</sup>

Received: 11 June 2015 / Accepted: 12 March 2016  
© Springer-Verlag Berlin Heidelberg 2016

**Abstract** In this study, we analyzed the influence of El Niño–Southern Oscillation (ENSO) on the spatio-temporal variability of droughts in Ecuador for a 48-year period (1965–2012). Droughts were quantified from 22 high-quality and homogenized time series of precipitation and air temperature by means of the Standardized Precipitation Evapotranspiration Index. In addition, the propagation of two different ENSO indices (El Niño 3.4 and El Niño 1 + 2 indices) and other atmospheric circulation processes (e.g., vertical velocity) on different time-scales of drought severity were investigated. The results showed a very complex influence of ENSO on drought behavior across Ecuador, with two regional patterns in the evolution of droughts: (1) the Andean chain with no changes in drought severity, and (2) the Western plains with less severe and frequent droughts. We also detected that drought variability in the Andes mountains is explained by

the El Niño 3.4 index [sea surface temperature (SST) anomalies in the central Pacific], whereas the Western plains are much more driven by El Niño 1 + 2 index (SST anomalies in the eastern Pacific). Moreover, it was also observed that El Niño and La Niña phases enhance droughts in the Andes and Western plains regions, respectively. The results of this work could be crucial for predicting and monitoring drought variability and intensity in Ecuador.

**Keywords** Standardized Precipitation Evapotranspiration Index (SPEI) · Drought · Ecuador · El Niño 3.4 · El Niño 1 + 2

## 1 Introduction

Drought is one of the main natural hazards affecting a variety of economic and natural systems. It is not just determined by a number of anthropogenic and natural factors, but also by the degree of vulnerability of different vegetation communities and human societies to water deficits. In addition, the risk of drought occurrence is closely related to a diversity of climate processes, such as the climatology of each region, including the spatial and temporal variability of climate variables, and different atmospheric circulation mechanisms (Schubert et al. 2004; Seager et al. 2005; Vicente-Serrano et al. 2011a).

Drought is among the most complex climatic phenomena (Wilhite 1993) due to the difficulties to quantify drought severity. In particular, a drought is characterized using their impacts on different systems (e.g., agriculture, water resources, ecology, forestry and economy), while there is actually no physical variable that can be measured directly to quantify droughts. In addition, droughts are difficult to pinpoint in time and space since it is very complex

✉ S. M. Vicente-Serrano  
svicen@ipe.csic.es

<sup>1</sup> Instituto Pirenaico de Ecología, Consejo Superior de Investigaciones Científicas (IPE–CSIC), Saragossa, Spain  
<sup>2</sup> Center for Climate Change, C3, Universitat Rovira i Virgili (URV), Tarragona, Spain  
<sup>3</sup> Centro Internacional para la Investigación del Fenómeno de El Niño (CIIFEN), Guayaquil, Ecuador  
<sup>4</sup> Water Desalination and Reuse Centre (WDRC), King Abdullah University of Science and Technology, Thuwal, Saudi Arabia  
<sup>5</sup> Department of Geography, Mansoura University, Mansoura, Egypt  
<sup>6</sup> Estación Experimental Aula Dei, Consejo Superior de Investigaciones Científicas (EEAD-CSIC), Saragossa, Spain  
<sup>7</sup> Environmental Physics Laboratory, Universidade de Vigo, Ourense, Spain

to identify the moment in which a drought starts or ends and also to quantify its duration, magnitude and spatial extent. Another important source of drought complexity is also associated with its multiscale character of drought, which is related to the different periods that exist from the arrival of water inputs to availability of usable resource in different natural systems and economic sectors (Changnon and Easterling 1989; McKee et al. 1993).

In tropical regions of South America, hydro-climatic hazards cause large social and economic impacts (Stillwell 1992; Hamilton et al. 2002, 2004). Intense precipitation events and floods have usually devoted the highest attention in the scientific literature given their adverse and drastic impacts on human casualties, infrastructure damaging and health epidemics (Lyon 2003; Mosquera-Machado and Ahmad 2007; Bourma and Dye 1997; Gagnon et al. 2002; Künzler et al. 2012). Nonetheless, droughts have received a relatively less attention in Northern South America, possibly due to high precipitation amounts experiencing little inter-annual variations and high soil water availability in the region. However, in past decades, these areas were also affected by strong drought events as a consequence of severe precipitation shortages (see for example, Marengo et al. 2008; Phillips et al. 2009; Lewis et al. 2011; Mo and Berbery 2011; Paredes and Guevara 2013). In this region, global warming processes may also induce an increase in the atmospheric evaporative demand, and thus increasing soil water stress and reducing the availability of water resources (Dai 2011, 2013). Over humid forests of South America, this mechanism has already been hypothesized as one of the causes of recent episodes of forest decay and increased tree-mortality (Jiménez-Muñoz et al. 2013; Vourlitis et al. 2014; Olivares et al. 2015) and forest fire (Román-Cuesta et al. 2014). All these features stresses the need for assessing the spatial and temporal behavior of droughts in these regions and improving the knowledge of the influence of different atmospheric mechanisms on this phenomenon.

Ecuador, a small country (283,560 Km<sup>2</sup>) located in northwest South America, shows a strong geographic and topographic diversity between the highlands, which correspond to the Andean chain with a south-north direction, the coastland plains in the west, and the Amazonian Jungle in the east. Topographical gradient is very strong, where it is possible to move from the sea level to peaks above 6000 m.a.s.l within a distance of <300 km. Drought episodes in Ecuador are linked to different atmospheric mechanisms, mainly the circulation in the Pacific and Atlantic regions (Poveda and Mesa 1997; Poveda et al. 2006; Haylock et al. 2006). Among them, El Niño–Southern Oscillation (ENSO) plays the main role in explaining climate variability in the country (Rossel et al. 1999; Rossel and Cadier 2009; Vuille et al. 2000a, b, 2003; Poveda et al.

2006). However, albeit the strong relief complexity, there are different atmospheric mechanisms that affect some regions of the country at different spatial scales (Rollenbeck et al. 2011; Rollenbeck and Bendix 2011). Given this topographic diversity, which causes different climate regimes in Ecuador (Bendix and Lauer 1992) and strong precipitation contrasts even at short distances (Buytaert et al. 2006; Celleri et al. 2007), it can be hypothesized that elevation gradients may control spatial and temporal variability of droughts, and can largely modulate the influence of atmospheric circulation processes across the country as well.

Earlier studies have stressed the complexity of the ENSO phenomenon in terms of the non-linear response of droughts to cold (La Niña) and warm (El Niño) phases in several regions of the world, including South America (Vicente-Serrano et al. 2011a). Other works have also reported a complex pattern of the ENSO, with different spatial configurations over the latest decades (e.g., Ashok et al. 2007; Weng et al. 2009; Yeh et al. 2014). This has enunciated the term “ENSO flavors” to refer the different spatial forms in which the ENSO occurs (Trenberth and Smith 2006; Lee and McPhaden 2010; Johnson 2013). Two main spatial configurations of the ENSO have been identified: a canonical eastern Pacific pattern and a recently identified central pattern, called as El Niño Modoki (Ashok et al. 2007). The climate response to these ENSO patterns is complex, with remarkable regional differences in the Pacific areas according to their influence on different atmospheric mechanisms in the region (e.g., Cai and Cowan 2009; Yoon et al. 2012; Dewitte et al. 2012; Tedeschi et al. 2013; Li et al. 2013; Córdoba-Machado et al. 2015). Drumond and Ambrizzi (2006) observed that the interannual variability of the boreal winter precipitation in Ecuador may be linked to the variations in the South American Monsoon System, which seems to be also related to the low frequency and the quasi-biennial components of the ENSO. Their results suggest that the displacement of the convection over Indonesia and western Pacific may contribute to the different responses in the precipitation observed during the ENSO events of the same signal. The spatial complexity and climate influence of these ENSO flavors probably interact with the complex drought behavior (including temporal evolution, spatial propagation and time-scales) and they are probably strongly affected by the complex orography of Ecuador. More recently, Córdoba-Machado et al. (2015) have analyzed the influence of canonical El Niño and El Niño Modoki on the spatial and temporal variability of precipitation in Columbia, showing a very different spatial and seasonal response to these patterns and also indicating how orography alters the ENSO effects in the country, in agreement with previous research by Poveda et al. (2011).

Studies suggest recent changes in the frequency of the different ENSO flavors, showing a higher frequency of the central El Niño events and a lower frequency of the Eastern El Niño phases in the last three decades (Lee and McPhaden 2010; Takahashi et al. 2011; Dewitte et al. 2012). These observed changes reinforce the need for knowing the response of droughts to different ENSO conditions in order to assess the possible impacts associated with the projected changes in the spatial configurations (Yeh et al. 2014), as well as the frequency and severity of cold and warm phases (Borlace et al. 2013; Taschetto et al. 2014).

The main objectives of this study are: (1) to analyze the spatial and temporal patterns of droughts in Ecuador, (2) to determine the influence of different ENSO indices and their intensity over the central and eastern parts of the Pacific region on different time-scales of drought severity and (3) to know the propagation of El Niño and La Niña phases on drought time-scales. Given that this study employs a high quality dataset of meteorological stations across Ecuador, which is available from the decade of 1960, assessing the complexity of the drought behavior in the region and their association with the ENSO variability and other atmospheric circulation processes could deepen our knowledge about the regional response of drought severity in Ecuador to the atmospheric circulation processes related to the ENSO.

To our knowledge, this is the first quantitative study of droughts in Ecuador that considers the complex topographic and climate characteristics of the country, providing a comprehensible explanation of drought variability in a region subjected to current climate change processes.

## 2 Data and methods

### 2.1 Data

#### 2.1.1 Meteorological data

The meteorological data have been provided by the “Instituto Nacional de Meteorología e Hidrología” (INAMHI) of Ecuador. Daily air temperature and precipitation time series for 50 stations in Ecuador (Fig. 1) were quality controlled with specifically designed software, which identified and removed gross measurement errors and identified and corrected transcription and data formatting problems. Following this screening procedure, we identified 22 stations (Table 1) with sufficient temporal coverage in the 1965–2012 period (for locations see Fig. 1). Given the low data availability in the INAMHI database, we tried to optimize all the available information. For this reason, although the Querochaca shows large data gaps in the temperature

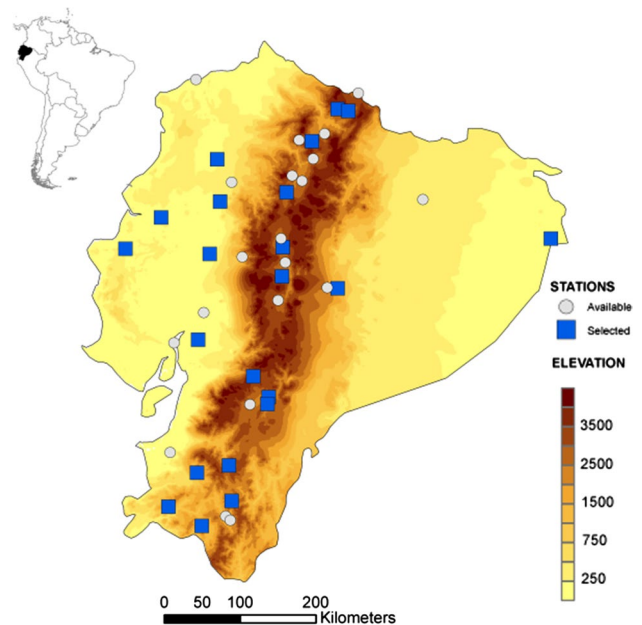


**Fig. 1** Study area and location of the meteorological stations used in this study. *Colour legend* represents changes in the elevation (in meters) of Ecuador. *Blue squared*: selected stations. *Gray circles*: non-selected stations

data, the precipitation series only shows the 21 % of data gaps, and given that the spatial variability of precipitation is much higher than temperature, we decided to include this station although the 40 % of the gaps were necessary to complete in the temperature series. This decision has not a noticeable influence in the obtained results (see below).

Monthly averaged values of daily maximum and minimum air temperature and monthly accumulations of daily precipitation were computed and homogenized using HOMER algorithm (Mestre et al. 2013). HOMER contains as a preliminary detection tool the pairwise algorithm described in Caussinus and Mestre (2004) and the two factors ANOVA model for correction presented by the same authors. This approach was identified as one of the best performing methods using the COST-HOME action benchmark datasets (see Venema et al. 2012 for a full evaluation of different homogenization approaches). HOMER also includes an extension of the pairwise detection algorithm based on Picard et al. (2011), which allows to simultaneously compare a set of stations and estimate the number and the positions of their breakpoints. Although the latter procedure could be applied in a fully automatic mode, the process was run semi-automatically, involving expert evaluation and the use of the very few available metadata.

Precipitation data was log-transformed before homogenization to improve the accuracy of break-point detection and only 11 very obvious breaks corresponding to five different stations were adjusted. For air temperature,

**Table 1** List of the 22 meteorological stations, their names, coordinates and elevation (in meters)

Code	Name	Latitude	Longitude	Elevation (m)	% Gaps precip.	% Gaps tmax.	% Gaps tmin.
M0003	IZOBAMBA	-0.366	-78.55	3058	1.1	1.4	1.4
M0004	RUMIPAMBA-SALCEDO	-1.02	-78.594	2685	19.7	19.9	20.1
M0005	PORTOVIEJO-UTM	-1.0375	-80.459	46	1.4	1.1	1.9
M0006	PICHILINGUE	-1.1	-79.461	120	0.7	0.5	0.9
M0007	NUEVO ROCAFUERTE	-0.916	-75.416	265	18.8	18.3	18.7
M0008	PUYO	-1.507	-77.943	960	6.2	6.5	6.5
M0025	LA CONCORDIA	0.026	-79.371	379	1.2	1.2*	1.4*
M0026	PUERTO ILA	-0.476	-79.338	319	1.8	1.9	2.5
M0031	CAÑAR	-2.551	-78.945	3083	1.9	2.5*	1.8*
M0033	LA ARGELIA-LOJA	-4.036	-79.201	2160	3.5	3.2	3.5
M0037	MILAGRO	-2.115	-79.599	13	0.9	1.1*	1.1*
M0102	EL ANGEL	0.626	-77.943	3000	5.5	7.2*	9.5*
M0103	SAN GABRIEL	0.604	-77.819	2860	4.0	3.3*	6.5*
M0105	OTAVALO	0.243	-78.25	2550	2.1	2.1*	2.5*
M0138	PAUTE	-2.8	-78.762	2194	5.3	5.5*	7.6*
M0139	GUALACEO	-2.881	-78.776	2230	10.0*	24.8*	23.4*
M0142	SARAGURO	-3.611	-79.233	2525	2.6*	4.6*	5.1*
M0146	CARIAMANGA	-4.333	-79.554	1950	4.0*	3.3*	7.9*
M0148	CELICA	-4.104	-79.951	1904	11.6*	12.3*	13.9*
M0162	CHONE-U.CATOLICA	-0.664	-80.036	36	8.6	7.6	9.3
M0180	ZARUMA	-3.698	-79.611	1100	7.7*	11.3*	27.1*
M0258	QUEROCHACA(UTA)	-1.367	-78.605	2865	21.1	40.7	40.1

The percentage of data gaps in the original series is also included and the series that contained temporal inhomogeneities are marked (\*)

maximum and minimum monthly temperature series were adjusted separately, but the accepted breaks for any of the two variables was incorporated in both. This procedure allows for monthly mean air temperature to be derived from both so that air temperature remains coherent. Again, a conservative approach was employed for the acceptance of breaks and only 12 stations needed the adjustment of 36 inhomogeneities. HOMER also completed missing values based on Equation 8 reported by Mestre et al. (2013).

### 2.1.2 Atmospheric and sea surface temperature information

Due to the intrinsic complexity of the ENSO phenomenon, there are different indices to quantify it, based on atmospheric or sea surface temperature (SST) data (Trenberth and Stepaniak 2001). In this study, we used two different indices to quantify the ENSO phenomenon, namely El Niño 3.4 Index and El Niño 1 + 2 Index, which were obtained from the SST dataset from the Hadley Centre UK (Rayner et al. 2003). El Niño 3.4 Index is obtained by averaging the SST in the central Pacific region (170°W, 5°S–120°W, 5°N) and normalized to 1971–2000 period. On the other hand, El Niño 1 + 2 records SST anomalies in the eastern Pacific region (90°W, 10°S–80°W, 0°S). The

Pearson's  $r$  correlation between the winter El Niño 3.4 and El Niño 1 + 2 is 0.78, which means that they only share the 60.8 % of the common variance in the period 1965–2012. Thus, the two indices record the specific behavior of the ENSO intensity in the central and east configurations.

El Niño events were defined by a boreal winter (December, January and February) El Niño 3.4 >1 or El Niño 1 + 2 indices >1, and La Niña events were defined by indices less than -1 and less than -0.8, respectively, considering the period 1965–2012. The thresholds were different for La Niña events in the two indices to have more representation of cold events considering the El Niño 1 + 2 index. Based on these criteria for El Niño 3.4 the winters of the years starting in January: 1966, 1973, 1983, 1987, 1992, 1995, 1998, 2003 and 2010 were classified as El Niño, and the winters of 1971, 1974, 1976, 1989, 1999, 2000, 2008 and 2011 were classified as La Niña. According to El Niño 1 + 2 the winters of 1973, 1983, 1987 and 1998 were classified as El Niño and the winters of 1968, 1971, 1974, 1975, 1976, 1981 and 2008 were classified as La Niña.

To determine the physical processes that explain the influence of ENSO on droughts, we also used data of SST at a spatial resolution of 1° from the Hadley Centre Sea Ice and Sea Surface Temperature data set (HadISST) for the region 165°W, 51°S–24°W, 34°N. Finally, we used data

from sea level pressure (SLP), and geopotential heights and vertical velocity ( $\omega$ ) at 1000, 925, 850, 700, 600, 500, 400 and 300 hPa. The positive (negative) vertical velocity means dominant descending (ascending) currents, denoting the intensity and surface extent of the convection processes in the region. This data was obtained from NCEP/NCAR reanalysis dataset at a spatial resolution of  $2.5^\circ$  (Kalnay 1996).

## 2.2 Analysis

### 2.2.1 Drought index calculation

To identify drought severity and variability, we used the Standardized Precipitation Evapotranspiration Index (SPEI). The SPEI was first proposed by Vicente-Serrano et al. (2010a) as an improved drought index that is especially suited for studies of the effect of global warming on drought severity. Like the Palmer Drought Severity Index (PDSI), the SPEI considers the effect of reference evapotranspiration on drought severity, but the multi-scalar nature of the SPEI enables identification of different drought types and drought impacts on diverse systems (Vicente-Serrano et al. 2012, 2013). Thus, the SPEI has the sensitivity of the PDSI in measurement of evaporative demand of the atmosphere (caused by fluctuations and trends in climatic variables other than precipitation), is simple to calculate, and is multi-scalar, like the Standardized Precipitation Index (SPI). Vicente-Serrano et al. (2010a, b, 2011b, 2012, 2015) and Beguería et al. (2014) provided complete descriptions of the theory behind the SPEI, the computational details, and comparisons with other drought indicators such as the PDSI and the SPI. Specifically, the SPEI is based on a monthly climatic water balance (P-ET<sub>o</sub>), which is adjusted using a 3-parameter log-logistic distribution. The values are accumulated at different time scales and converted to standard deviations with respect to average values.

The SPEI is perfectly comparable in time and space, and across different timescales. Thus, the same SPEI values occur with the same frequency in all regions of the world, independent of the climate characteristics of the region. This index provides objective information on climatic drought conditions, as it relies only on climate data. It is also able to identify climate change processes related to changes in precipitation and the atmospheric evaporative demand since the SPEI is equally sensitive to these two variables (Vicente-Serrano et al. 2015).

To calculate SPEI, it is necessary to determine the atmospheric evaporative demand (AED), which is heavily influenced by physical factors and involves a combination of radiative and aerodynamic components (McVicar et al. 2012 and references therein). These components were combined by Penman (1948), who developed an equation to

measure the evaporative demand of the atmosphere using meteorological data (wind speed, solar radiation, relative humidity and air temperature). Nevertheless, a common problem in estimating the AED is the absence of long time series of wind speed, solar radiation and relative humidity, which is the case for Ecuador. For this reason, we used a simplified equation developed by Hargreaves and Samani (1985), which only requires information on maximum and minimum air temperatures, and the extraterrestrial solar radiation, and it provides very similar estimates to those more complex methods like the FAO-56 Penman–Monteith equation (Droogers and Allen 2002; Hargreaves and Allen 2003). Using precipitation and AED estimates for the 22 available meteorological stations in Ecuador, we calculated the SPEI at time scales between 1- and 48-month between 1965 and 2012.

### 2.2.2 Classification of drought patterns

We obtained homogeneous drought patterns using an S-mode principal component analysis (PCA) (Richman 1986), which was applied to the 12-month SPEI series as representative of general SPEI evolution in Ecuador, to obtain the main modes of temporal variability of droughts. The PCA procedure has been widely applied in climatological studies (e.g. Jolliffe 1986, 1990; von Storch and Zwiers 1999; Richman 1986; Huth 2006). The uncorrelated variables obtained are termed principal components (PCs) and consist of linear combinations of the original variables.

Typically the complexity of the structure of each consecutive PC pattern increases (Richman 1986). Therefore, a common practice is to find an alternative set of vectors, which have a much simpler structure. This process is referred to as rotation. Rotation conserves the total variance of the components selected for rotation but redistributes it at the expense that successive maximization of variance is lost (Jolliffe 1986). Here the number of components selected for rotation was based on the criterion of an eigenvalue  $>1$ , and the components were rotated using the varimax method, selecting the correlation matrix to efficiently represent the variance (Barry and Carleton 2001). Performing a rotation with varimax retains orthogonality in the principal component time series but not the spatial patterns (Mestas-Núñez 2000). Nevertheless, the obtained drought Varimax Patterns (VPs) are less affected by domain dependence, have a smaller sampling error and they are more stable and physically robust than unrotated patterns (Richman 1986).

### 2.2.3 Relationship between drought indices and the ENSO

We correlated monthly SPEI at time scales of 1-, 3-, 6- and 12-month in each one of the 22 meteorological stations

with monthly series of El Niño 3.4 and El Niño 1 + 2 at the same time scales of 1-, 3-, 6- and 12-month (averaging the El Niño indices over the past  $n$  months). The significance of correlations was set at  $p < 0.05$ . We also calculated for each station the monthly averages of the 1- to 48-month SPEI corresponding to El Niño and La Niña episodes, identified from El Niño 3.4 and El Niño 1 + 2 indices (see Sect. 2.1.2) and the years before and after these events. These months could correspond to other conditions (e.g., El Niño in 1973 was followed by La Niña in 1974, and the same is observed in 2010 and 2011). The results were also obtained from the general SPEI series resulted from the VPs, described in Sect. 2.2.2, since these series are representative of large regions and they record the general SPEI anomalies in the country corresponding to El Niño and La Niña events. We used the non-parametric Wilcoxon-Mann-Whitney test (Siegel and Castelan 1988) to determine whether the SPEI at different time scales reflected significant humid or dry conditions during El Niño or La Niña events obtained from both indices. The SPEI values in each one of the months of El Niño/La Niña years were compared with the values of the SPEI for the months of normal years and those with the opposite sign. Thus, to determine the role of the El Niño years the SPEI values during La Niña years were added to the SPEI values during normal years, and vice versa. The significance level was defined as  $p < 0.05$ .

#### 2.2.4 Drought connection with SST and atmospheric circulation anomalies

To determine the driving mechanisms of the influence of ENSO on drought in Ecuador, in terms of El Niño 3.4 and El Niño 1 + 2 indices, and the possible spatial differences in the influence of these indices, we correlated the monthly 1-month SPEI of the main drought VPs with the gridded SST and the SLP and 500 hPa heights over the selected spatial domain (see Sect. 2.1.2). Regions with significant correlations were set as  $p < 0.05$ . These patterns show months of the year and regions in which these variables have an impact on 1-month SPEI anomalies. Obviously, the accumulation and temporal propagation of these anomalies will cause drought conditions, whose severity will be proportional to the monthly anomalies. In addition, we calculated correlation between monthly drought VPs obtained in the analysis described in Sect. 2.2.2, with the geopotential height and vertical velocity at different geopotential levels. For a graphical representation, we showed the correlations in a W-E profile between  $-170^\circ\text{E}$  and  $-70^\circ\text{E}$  at  $1^\circ\text{S}$  of latitude. We also calculated the anomalies of geopotential height and vertical velocity at different geopotential levels corresponding to El Niño and La Niña events identified with El Niño 3.4 and El Niño 1 + 2 indices, and also the

average SPEI anomalies corresponding to the three most arid years (negative annual SPEI values) and the three most humid years (positive annual SPEI values) recorded in each VP. Significant differences in the geopotential height and vertical velocity between El Niño/La Niña phases and between the humid/dry periods and the rest of years were obtained by means of the Wilcoxon–Mann–Whitney test.

## 3 Results

### 3.1 Patterns of drought variability

We observed strong differences in the evolution of droughts in Ecuador. The analysis applied to the 12-month SPEI series allowed to extract three VPs of drought evolution (Fig. 2), which explain almost 72 % of the total variance. VP1 represents the 36.6 % of the total variance and shows main drought patterns identified between 1975 and 1980, 1985–1993, 2002–2004 and a short but very intense period in 2010. This drought evolution is representative of the Andean chain that crosses Ecuador from North to South. VP2 contributes to 28.6 % of the total variance and temporal evolution is characterized by strong drought episodes in 1968–1969 and between 1978 and 1983. Since 1985 the drought episodes were characterized by low magnitude and no relevant changes. This evolution is representative of the Western plains close to the Pacific Ocean. Finally, VP3 only represents 6.7 % of the total variance and it represents the evolution of one observatory eastward of the Andes in which strong droughts were recorded in 1980, 1993–2000 and 2011–2012. For further analysis we have only retained the first two VPs, which represent 65.2 % of the total variance. The precipitation regimes are quite different between these two regions (Fig. 3). The Andean chain does not show strong precipitation seasonality, with maximum values recorded in March–April and October–December, and minimum values in July–September. On the contrary, the Western Plains show strong precipitation seasonality, with marked humid (December to May; 1360 mm on average) and dry seasons (June to November; 160 mm on average). In opposition to precipitation, seasonal and interannual variability of the ETo is very low both in the Andes and the Western Plains.

### 3.2 Correlations between droughts and ENSO

The clear differences in the drought evolution between the Western plains and the Andean chain are related to the existing differences in the ENSO influence on droughts. Figure 4 shows the correlations between the monthly El Niño 3.4 index and the 1-month SPEI during the 12 months of the year, but also between average 3-, 6- and 12-month

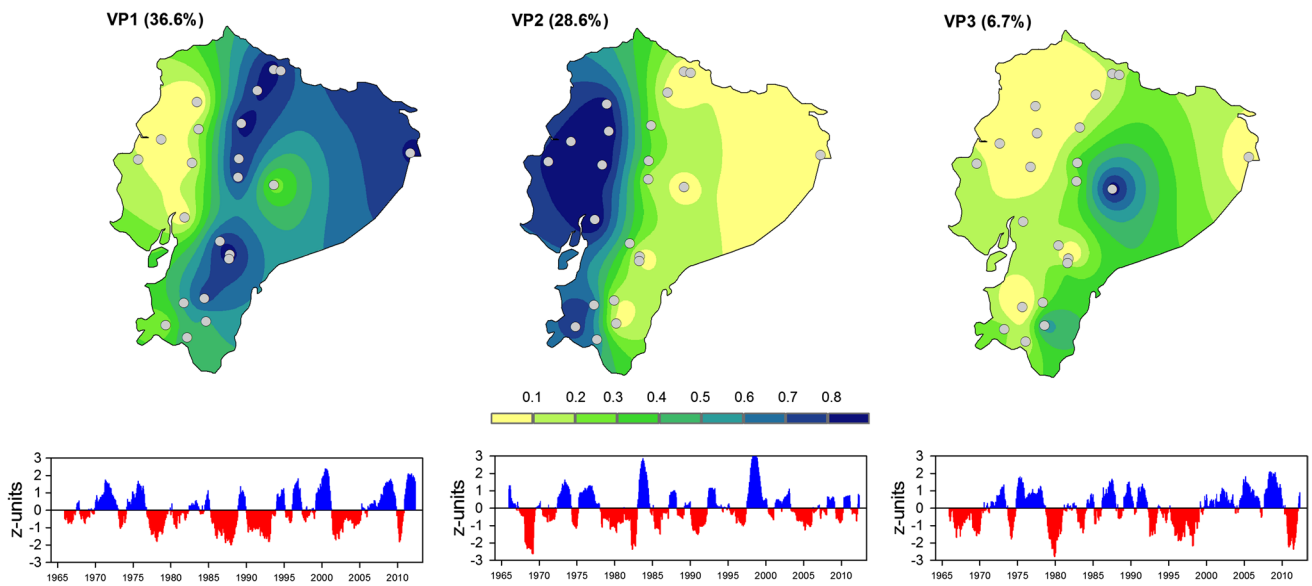


**Fig. 2** Top maps are the spatial distribution of the loadings from the obtained Varimax Patterns and *bottom plots* correspond to the time series of the scores, which represent the general evolution of the 12-month SPEI in each one of the three regions

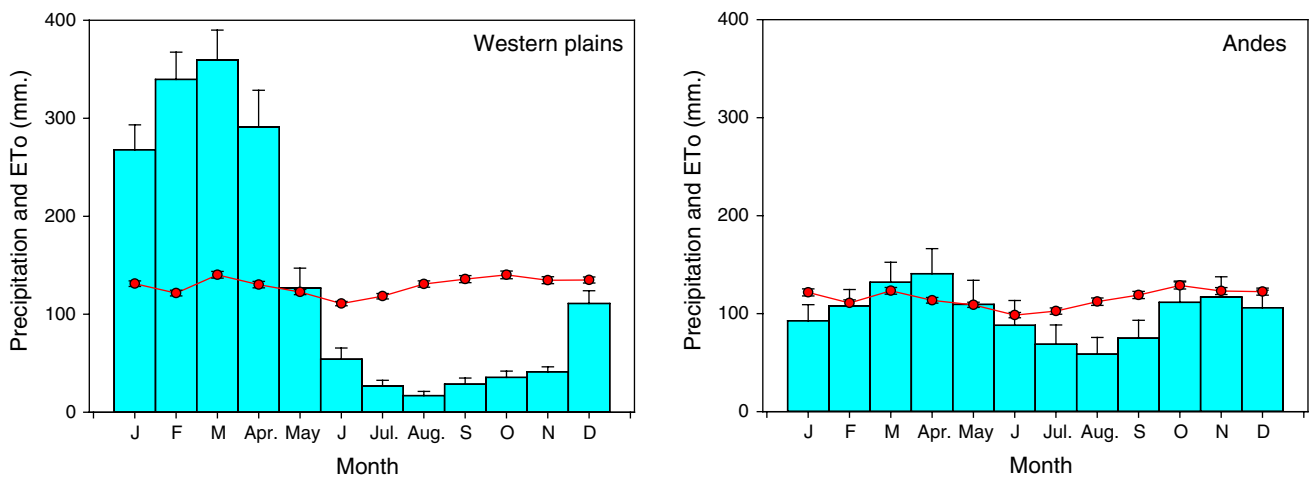


**Fig. 3** Average monthly precipitation (*blue bars*) and ETo (*red line*) in the Andes and the Western Plains. *Vertical bars* represent the standard error of the average

El Niño 3.4 index (e.g., the average of current month and previous 2 months for 3-month time-scale) and the 3-, 6- and 12-month SPEI. Between January and March there is a negative and significant correlation between the 1-month El Niño 3.4 index and the 1-month SPEI in the meteorological stations located in the Andean chain; on the contrary, in the plain areas close to the Pacific Ocean correlations are positive, but non-statistically significant. It means that warm SST conditions in the central Pacific region favors dry conditions in the Andean chain. In April and May, the stations located in the Western plains show positive and significant correlations with El Niño 3.4, whereas the Andean region

do not show significant correlations. From June to August the spatial pattern changes and correlations tend to be negative throughout the entire country, but only significant in the Andean chain. From September to December correlations are mostly non-significant in the whole area. At time scales of 3- and 6-months, the negative correlations found at the 1-month time scale in the Andes in some months of the year are also observed. At the 6-months, it is also evident how the SPEI series in the stations located in the Western plains are positively and significantly correlated to the El Niño 3.4 index. It means that, in the Western plains, warm SST conditions in the central Pacific favor humid

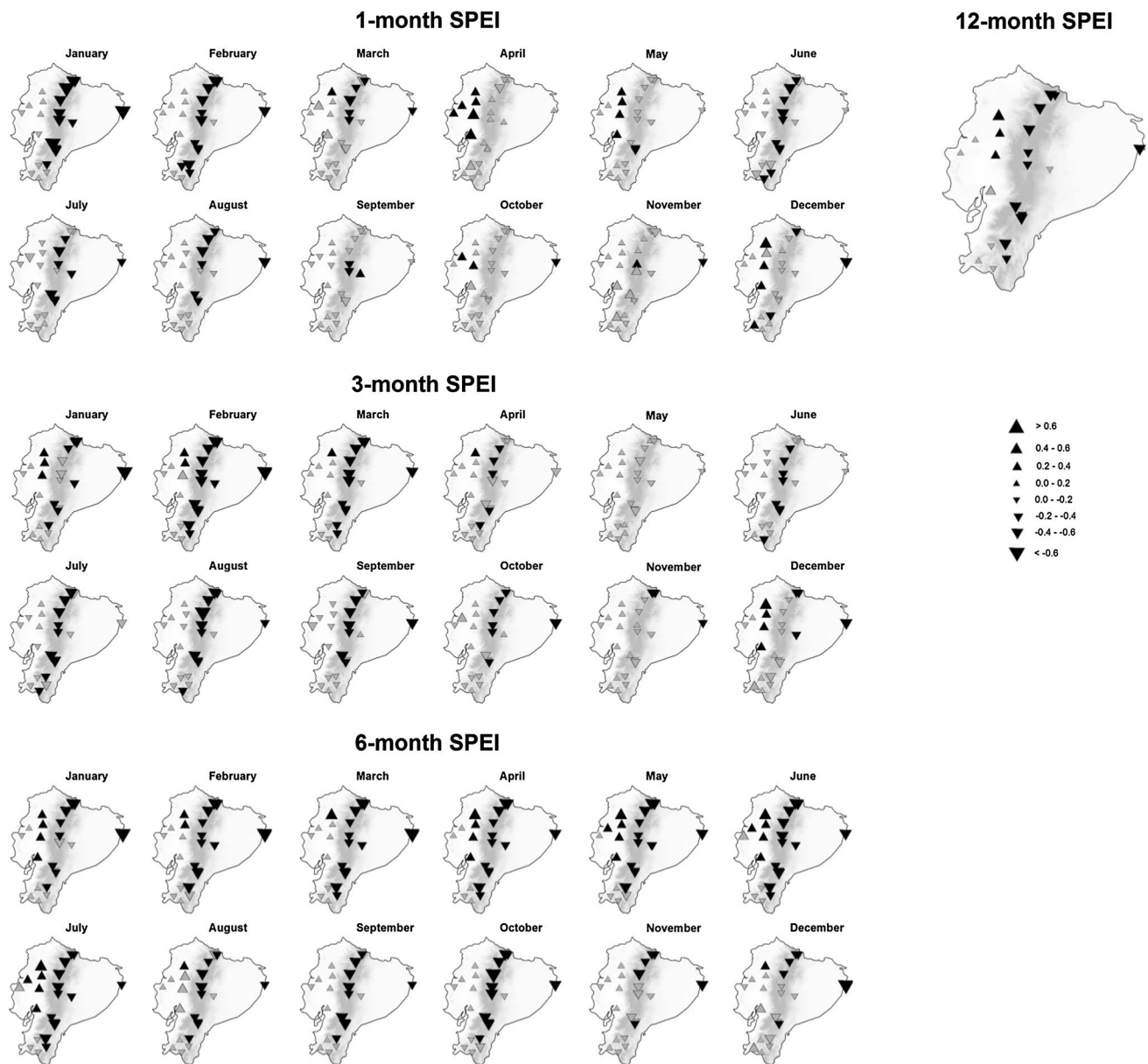


**Fig. 4** Spatial distribution of monthly correlations between the 1-month SPEI and 1-month NINO3.4 index, between 3-month SPEI and 3-month NINO3.4 index, between the 6-month SPEI and

6-month NINO3.4 index and between 12-month SPEI and 12-month NINO3.4 index. Significant correlations are in *black*

conditions, which is the opposite to that found in the Andes. The annual pattern (12-month SPEI) confirms this behavior demonstrating a very different response of droughts time-scales to El Niño 3.4 index between the Andes and the Western plains.

In the Andes, droughts would be favored by warm SST (El Niño) in the central Pacific region, but in the Western plains the drought episodes are more related to cold SST (La Niña) in the same Pacific region. Figure 5 also shows contrasted differences in the correlations of the SPEI and El Niño 1 + 2 Index between the Andes and the Western

plains in different months of the year and time-scales. The sign of the correlation coefficients is similar to that found for El Niño 3.4: positive in the Western plains and negative in the Andean chains. Nevertheless, the magnitude and signification of correlations are very different. Considering El Niño 1 + 2 Index positive correlations in the Western plains are dominantly significant, whereas in the Andes correlations are dominantly non-significant, with the exception of June. The pattern is reinforced considering 3-, 6- and 12-month SPEI, which demonstrate that drought episodes in the Western plains are better determined by

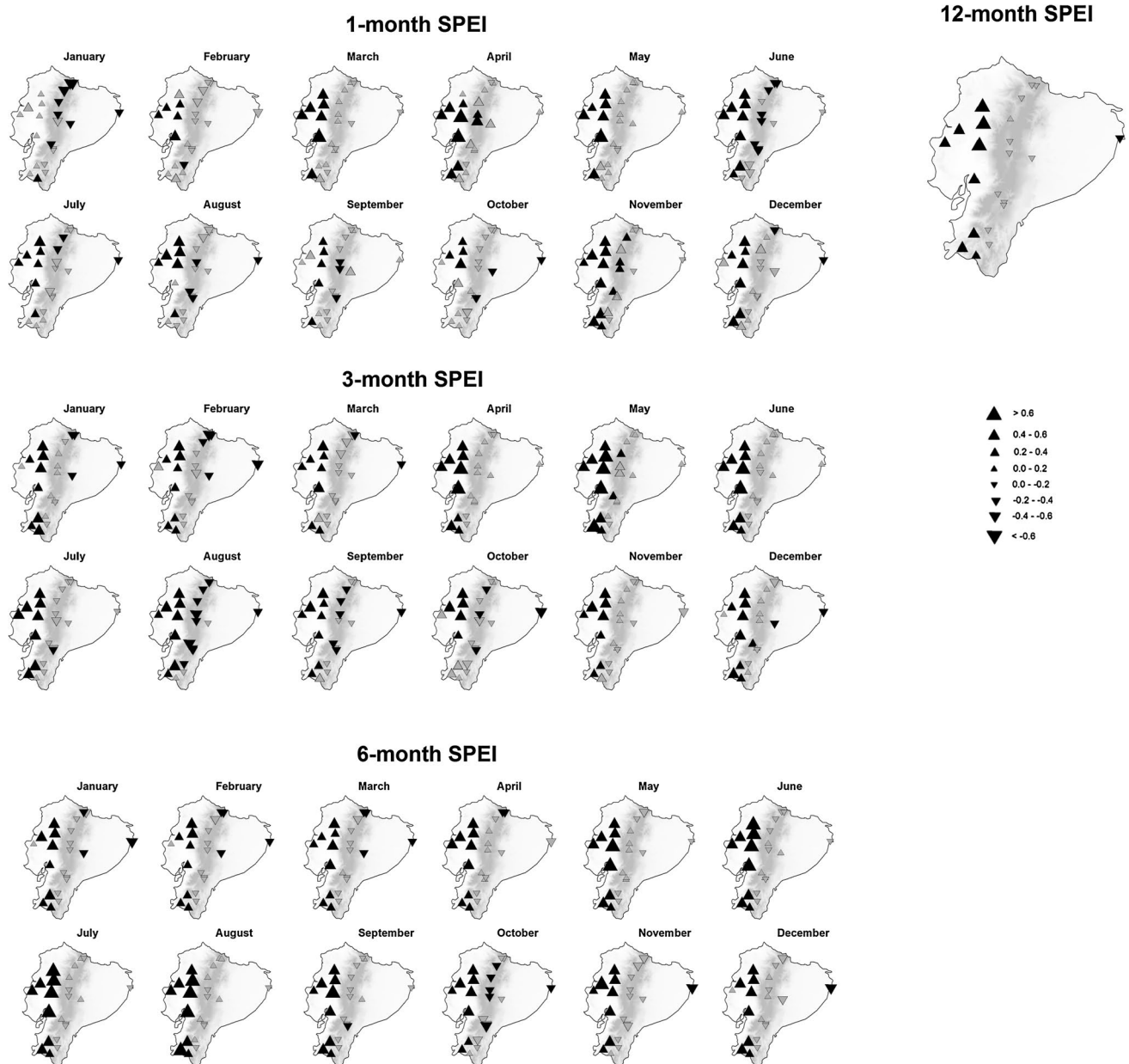


**Fig. 5** Same as Fig. 5, but for the NINO 1 + 2 index

cold SST conditions (La Niña) in the Eastern Pacific than in the central Pacific region, and the opposite is found for the Andes.

The strong but complex influence of ENSO in Ecuador suggests that the occurrence of warm (El Niño) and cold (La Niña) phases may drive the occurrence of droughts at different time-scales in different parts of the country, although slight differences are obtained between using El Niño 3.4 or El Niño 1 + 2 indices. Figure 6 shows the average 1- to 48-SPEI anomalies during the El Niño and La Niña years obtained from the El Niño 3.4 Index in the Andes (VP1) and the Western plain region (VP2). The SPEI at the different

time-scales are calculated from the regional series of the climatic water balance (precipitation minus reference evapotranspiration) in both regions according. The months of the identified El Niño and La Niña years (see Methods section) correspond to the framed months, but also the 12 months before and after the ENSO events are used to calculate the average anomalies. In the Andes, during La Niña, the SPEI is dominantly positive and significantly different to the rest of the years in different months of the year and SPEI time-scales. La Niña signal is very strong in this region; thus very high average positive anomalies (>1) are found at time-scales from 5- to 24-months but also during the previous

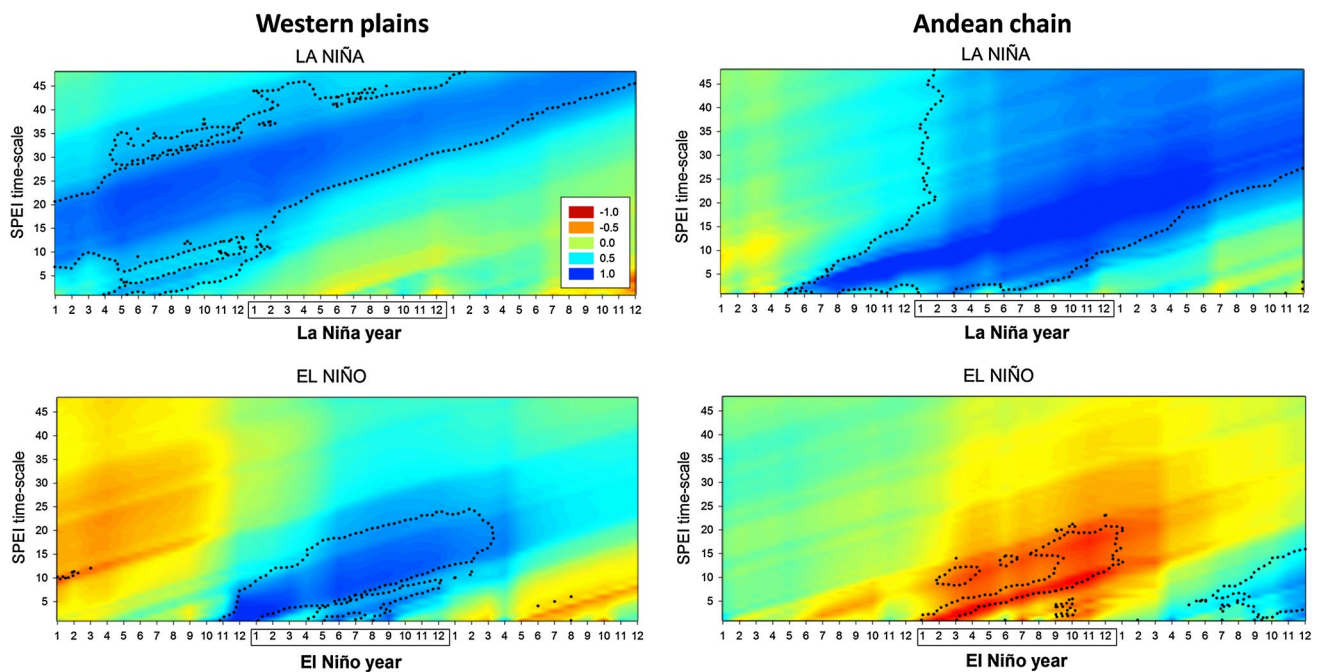


**Fig. 6** Average 1- to 48-month SPEI anomalies corresponding to El Niño and La Niña phases from El Niño 3.4 index. *Dotted lines* frame significant differences in the average SPEI anomalies between El

Niño or La Niña years and the rest of the years following the Wilcoxon–Mann–Whitney test

and following year. The positive anomalies during La Niña years seem to be an early precursor of the effects of the cold phase since significant positive anomalies of SST in the El Niño 3.4 region are found since June of the previous year (Vicente-Serrano et al. 2011a, b). Thus, the positive anomalies of SPEI in the Andes, recorded on short time-scales during the previous months to the ENSO year, propagate in the form of longer time-scales during La Niña year but also the following year, which indicates general humid conditions on a long time-scale. On the contrary, during El Niño years, the SPEI averages are dominantly negative. This is indicative of drought conditions, but these are mainly recorded at short time-scales. In any case, the drought response to El Niño years in the Andes shows a lower magnitude than the humid response to La Niña years, which suggests a clear asymmetry in the response to El Niño and La Niña phases in the central Pacific. On the other hand, the pattern of SPEI response to El Niño and La Niña years identified from El Niño 3.4 index is very different in the Western plains (VP2). La Niña years record humid conditions at long SPEI time-scales, as a consequence of the propagation of the humid conditions of the year before La Niña. On the contrary, negative SPEI values are recorded at short time-scales, although the magnitude of these anomalies is low and there are not significant differences with the rest of the years. During El Niño years there are positive SPEI anomalies, which are significantly different to the rest of the years. The positive SPEI anomalies are identified at short time scales at the

beginning of the El Niño phases and propagated to longer (10–20 months) during the entire El Niño year.

The pattern of response to El Niño 1 + 2 cold and warm phases is very different to that showed for El Niño 3.4 (Fig. 7). There are not clear patterns in the SPEI response of the Andes to La Niña and El Niño episodes obtained from El Niño 1 + 2, with non-significant SPEI anomalies in response to these events. Nevertheless, in the Western plains (VP2), during El Niño 1 + 2 cold and warm phases there are SPEI anomalies significantly different to the rest of years. Although the number of years identified as La Niña with El Niño 1 + 2 events is low (3), we have found dominant negative SPEI values at different time-scales and months during La Niña 1 + 2 events in the Western plains, but the differences are not dominantly significant different to the rest of the years, given the low number of years considered. Nevertheless, the response of the Western plains to El Niño 1 + 2 events is strong, showing general humid conditions, which are significantly different in different months of the year and SPEI time-scales to the rest of the years.

### 3.3 Physical drivers explaining the spatial differences in the influence of ENSO on droughts

Although the drivers of drought variability between the Andean areas and the Western plains seem to be highly connected to the ENSO phenomenon, they are responding

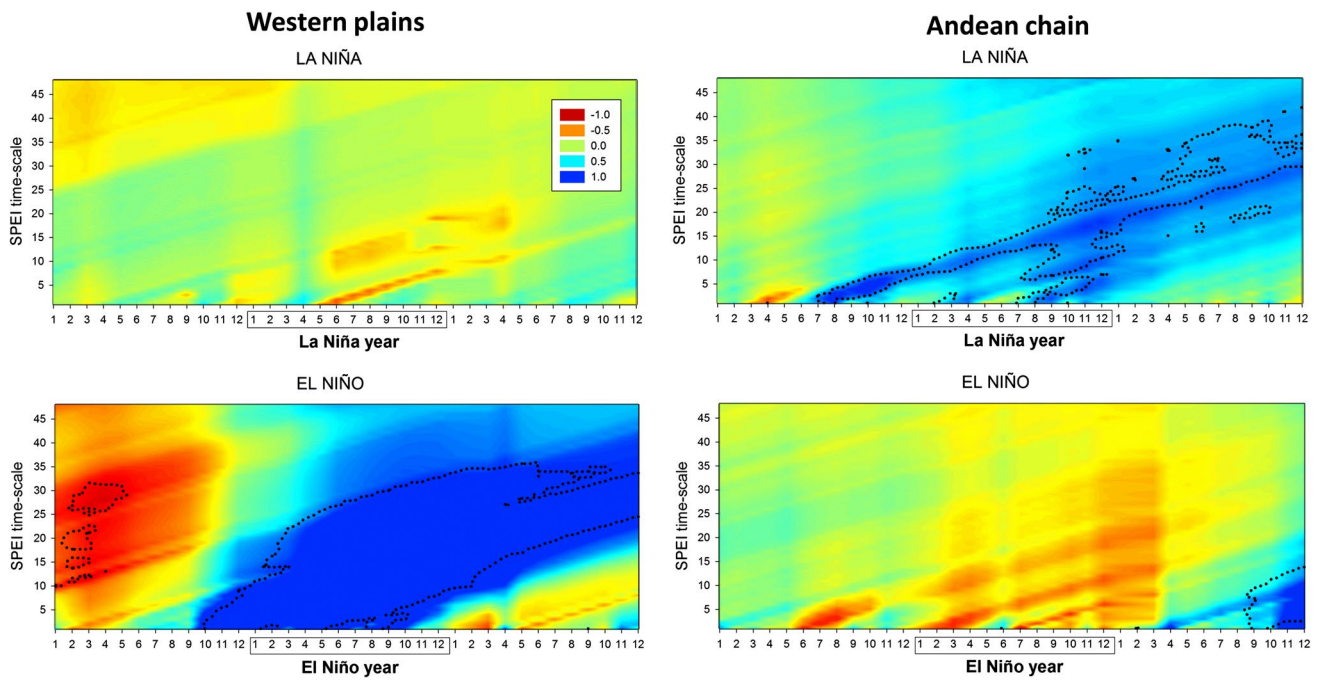


**Fig. 7** Average 1- to 48-month SPEI anomalies corresponding to El Niño and La Niña phases from El Niño 1 + 2 index. *Dotted lines* frame significant differences in the average SPEI anomalies between

El Niño or La Niña years and the rest of the years following the Wilcoxon–Mann–Whitney test

to different mechanisms that explain the complex and the different influence of the ENSO intensity in the central (El Niño 3.4) and eastern (El Niño 1 + 2) regions. Figure 8 shows that the Pacific regions in which SST correlate with the SPEI in the Andes (VP1) and Western plains (VP2) are very different. The SPEI values for the monthly 1-month VP1 show negative and significant correlation with the SST in a region of the central equatorial Pacific Ocean. This is clearly recorded in January and February and between June and September. Warm (cold) SST in the central Pacific shows a clear connection with dry (humid) conditions in the Andean region during these months. On the contrary, monthly 1-month SPEI in the Western coastal plains shows a very different correlation pattern with SST in the Pacific region. There are positive and significant correlations in the eastern Pacific region closest to the Ecuador coastland, which extend to large areas of the equatorial Pacific in April, May, November and December and resembling the spatial pattern of the canonical El Niño. It means that dry (humid) conditions in the Western plains are favored by cold (warm) SST in this region. Thus, this analysis indicates that SPEI variability in both regions shows a clear connection with SST anomaly, but the Andes is connected to the central Pacific SST anomalies area and the Western plains are linked to the SST in the eastern Pacific.

The influence of the SST anomalies in different Pacific regions in areas of Ecuador separated only by 200 km is

clearly connected with the coupled ocean–atmosphere processes associated with different ENSO configurations, modulated by the effect of the relief. In the Andes (VP1) there is no significant correlation between the SPEI and SLP over Ecuador, but evident significant correlations are found between the SPEI and SLP over the central Pacific region. On the contrary, in the Western plains there are negative and significant correlations between the SPEI and the SLP values over Ecuador, which is observed during several months of the year. Figure 9 shows the monthly correlations of 1-month SPEI series corresponding to Varimax Pattern 1 (Andes) and 2 (Western plains) with the geopotential levels at different heights in a profile between 160°W and 70°W at 1°S. The figures contain the relief of Ecuador, which is characterized by a “wall” of more than 4000 m elevation at 60°W. The Andes would show an influence of the pressure anomalies in the upper levels as a consequence of high elevation. Positive (negative) SPEI values in the Western plains are favored by negative SLP anomalies in the eastern equatorial Pacific region, which could be hypothetically associated with atmospheric circulations enhancing convective processes in the region, driven by SST conditions in the Eastern Pacific region. On the contrary, in the Andes the results show that the correlation is negative and statistically significant with geopotential levels at high elevations in most months of the year. The SLP variability associated with SST anomalies in the central Pacific affects the SPEI

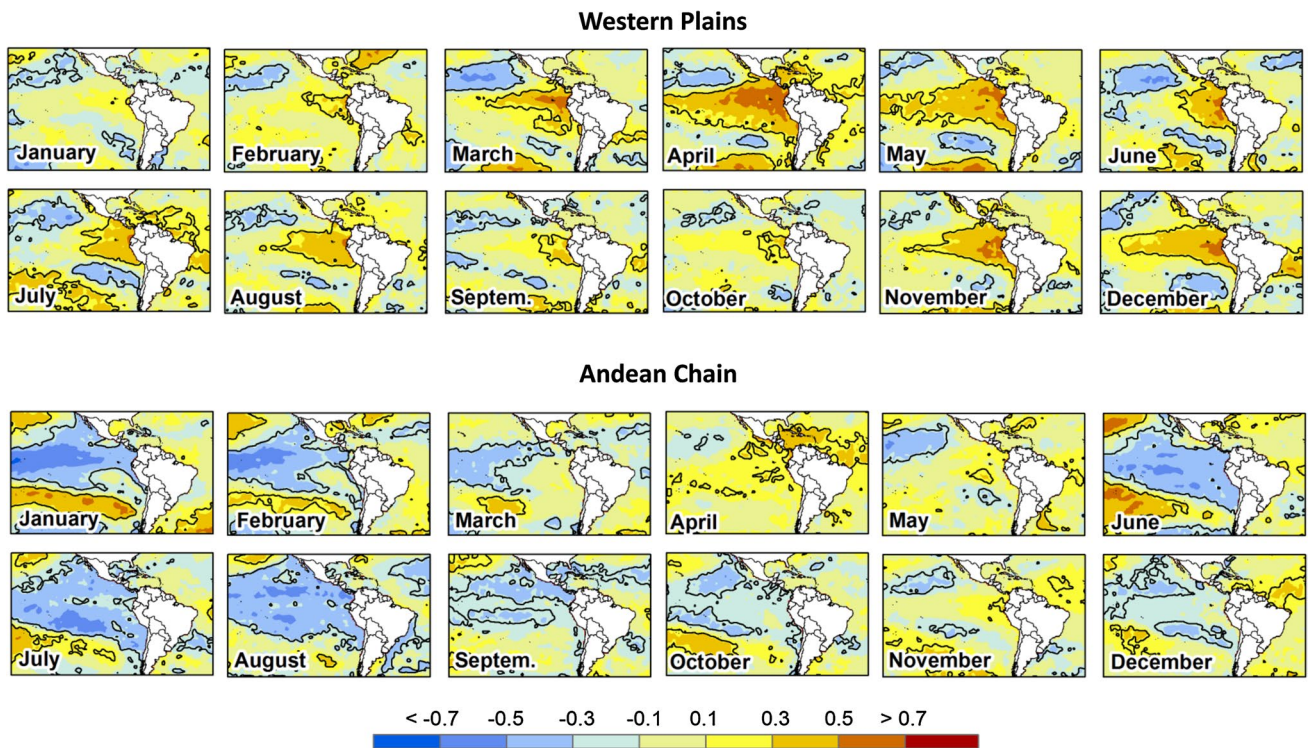


**Fig. 8** Monthly correlation between 1-month SPEI corresponding to the evolution of the Andean Chain (VP1) and the Western Plains (VP2) and the Sea Surface Temperature. *Black lines* isolate regions with significant correlations

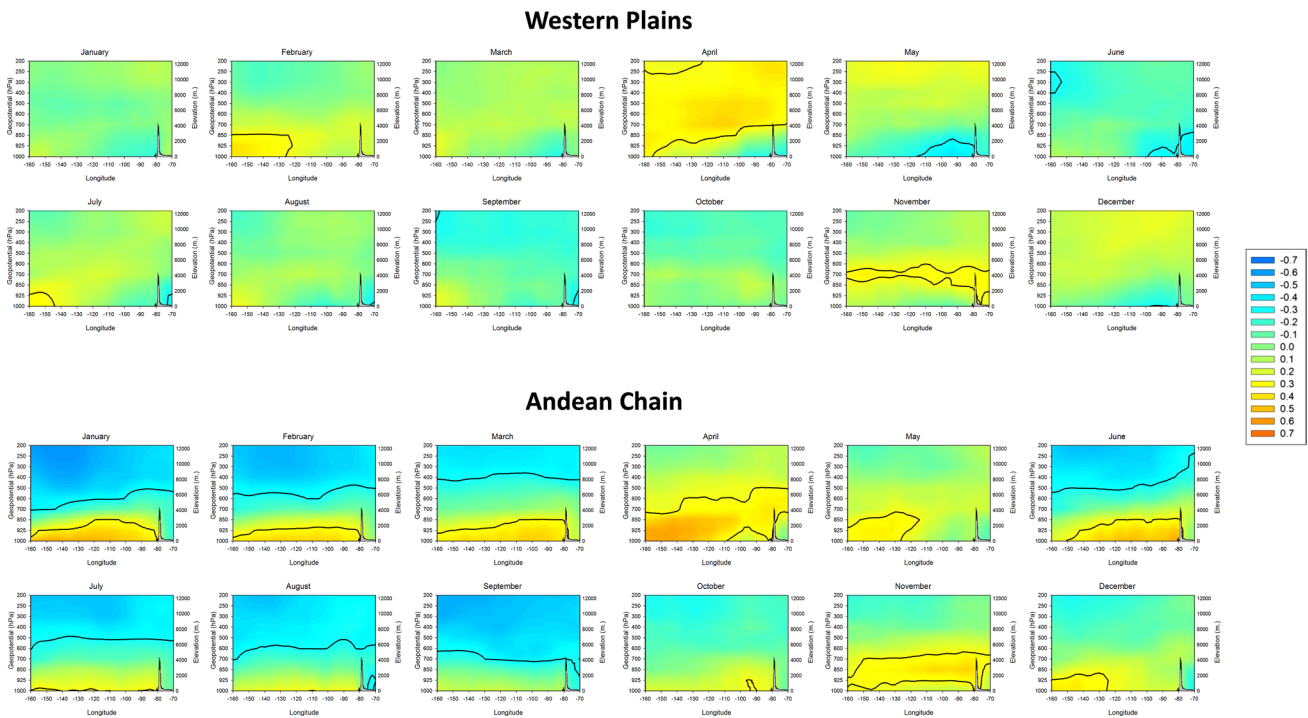


**Fig. 9** Monthly correlation between 1-month SPEI corresponding to the evolution of Varimax Pattern 1 (Andean Chain) and Varimax Pattern 2 (Western Plains) and Geopotential at different heights in

a profile between  $-160^{\circ}\text{E}$  and  $-70^{\circ}\text{E}$  at  $-1^{\circ}\text{S}$ . *Black lines* isolate regions and levels with significant correlations. The topography of the Andean chain is represented for facilitating the interpretation

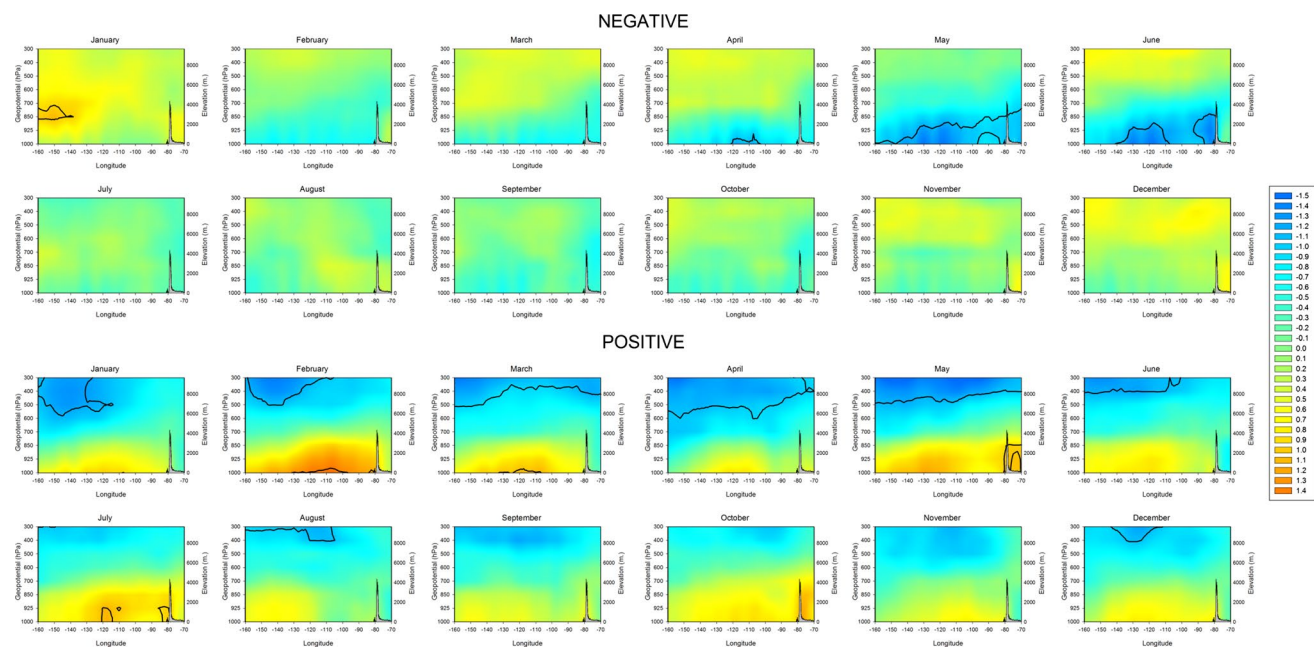


**Fig. 10** Monthly geopotential height anomalies corresponding to the three most humid (1974, 1999, 2008) and dry years (1985, 1987, 1992) in the Andean region (Varimax Pattern 1) in a profile between

–160°E and –70°E at –1°S. *Black line* isolates heights and regions in which the geopotential anomalies are significantly different to the rest of the years

variability in the Andes by means of propagation throughout the mid-troposphere. There are negative and significant correlations along a large band around the Equator, indicating that negative (positive) height anomalies cause positive (negative) SPEI values during more than half of the year. This connection explains why the region shows significant correlations with the SST and SLP of the central Pacific region, which is thousands of kilometers west of Ecuador. The SST anomalies in El Niño 3.4 region (central Pacific) would be transferred vertically to the middle and upper troposphere and propagated spatially by means of the Walker circulation, thus affecting the Andean region in Ecuador. Nevertheless, the influence of the mid- and upper-atmospheric circulation variability shows clearly a nonlinear behavior that would explain the different response of the SPEI of the Andes to the El Niño 3.4 warm and cold phases. The influence of the high elevation geopotential heights anomalies in the Andean region is mainly linked to positive (humid) SPEI values instead to negative (dry) conditions (Fig. 10). On the contrary, SPEI and mid and upper troposphere fields do not show significant correlations for the Varimax Pattern 2, indicating that the mid-troposphere variability does not influence significantly the SPEI variability in the Western plains of Ecuador.

Therefore, although it could be affirmed that drought variability in both regions of Ecuador are related to the ENSO, the ENSO flavors and the physical mechanisms that explain the effect are very different, and closely related to

the coupled ocean-atmospheric circulation processes and mainly to the existing topographical gradients in Ecuador. The average geopotential height anomalies during the three most humid years in the Andes show negative values, which are statistically different to those recorded during the rest of years. On the contrary, the three driest years do not show clear geopotential anomalies in the upper levels. In any case, we identify that El Niño phases show significant positive geopotential height anomalies during most months of the year (Fig. 11); the most intense being recorded during the humid season. This also shows that although El Niño 3.4 warm phases also cause negative and significant geopotential height anomalies near the surface, these do not affect the Andean region given high elevation of the region and no connection with SLP.

The geopotential height anomalies at different levels corresponding with the most positive (humid) and negative (dry) years recorded in the Western plains (Fig. 12) show very different pattern to that observed for the Andes. In this region, the most humid years show strong positive geopotential height anomalies at higher elevation levels, but negative anomalies at the surface level, that although they are non-significant, they are more intense over the Western plains. This pattern closely resembles the geopotential height anomalies observed during El Niño 1 + 2 index during several months of the year (Fig. 13), in which geopotential heights near the surface clearly show negative anomalies. On the contrary, during the dry phases the pattern in

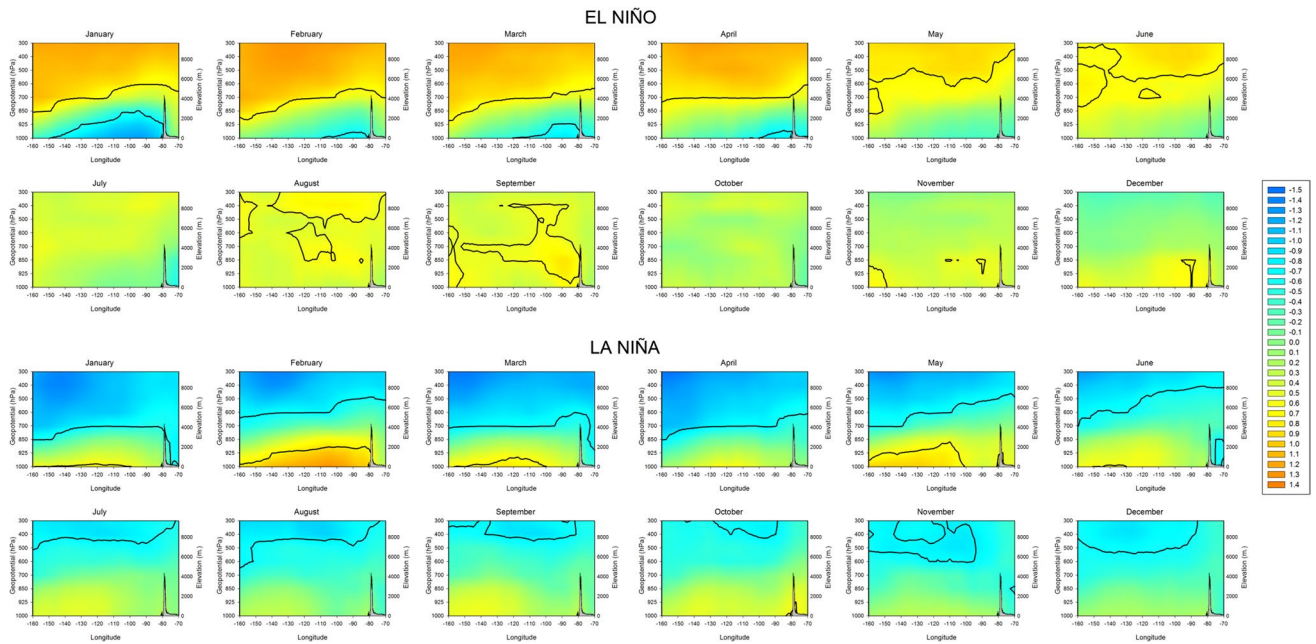


**Fig. 11** Monthly geopotential height anomalies corresponding to El Niño and La Niña phases from El Niño 3.4 Index in a profile between  $-160^{\circ}\text{E}$  and  $-70^{\circ}\text{E}$  at  $-1^{\circ}\text{S}$ . *Black line* isolates heights and regions

in which the geopotential anomalies are significantly different to the rest of the years

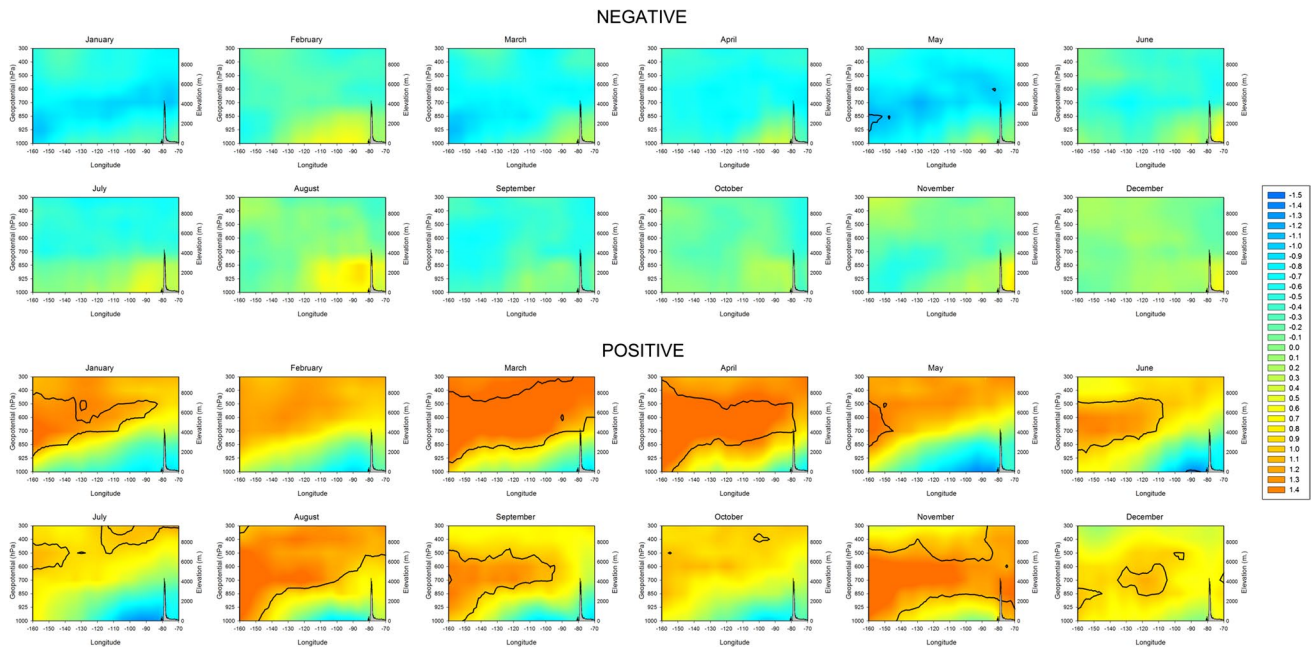


**Fig. 12** Monthly geopotential height anomalies corresponding to the three most humid (1983, 1997, 1998) and dry (1968, 1985, 1990) years in western plain region (Varimax Pattern 2) in a profile between

$-160^{\circ}\text{E}$  and  $-70^{\circ}\text{E}$  at  $-1^{\circ}\text{S}$ . *Black line* isolates heights and regions in which the geopotential anomalies are significantly different to the rest of the years

geopotential anomalies is not clear, although there is a domain of positive anomalies for geopotential upper levels and negative anomalies near the surface in agreement to

that observed during La Niña years. The clear differences in SLP and geopotential anomalies during El Niño 1 + 2 warm and cold phases, which is even more evident than

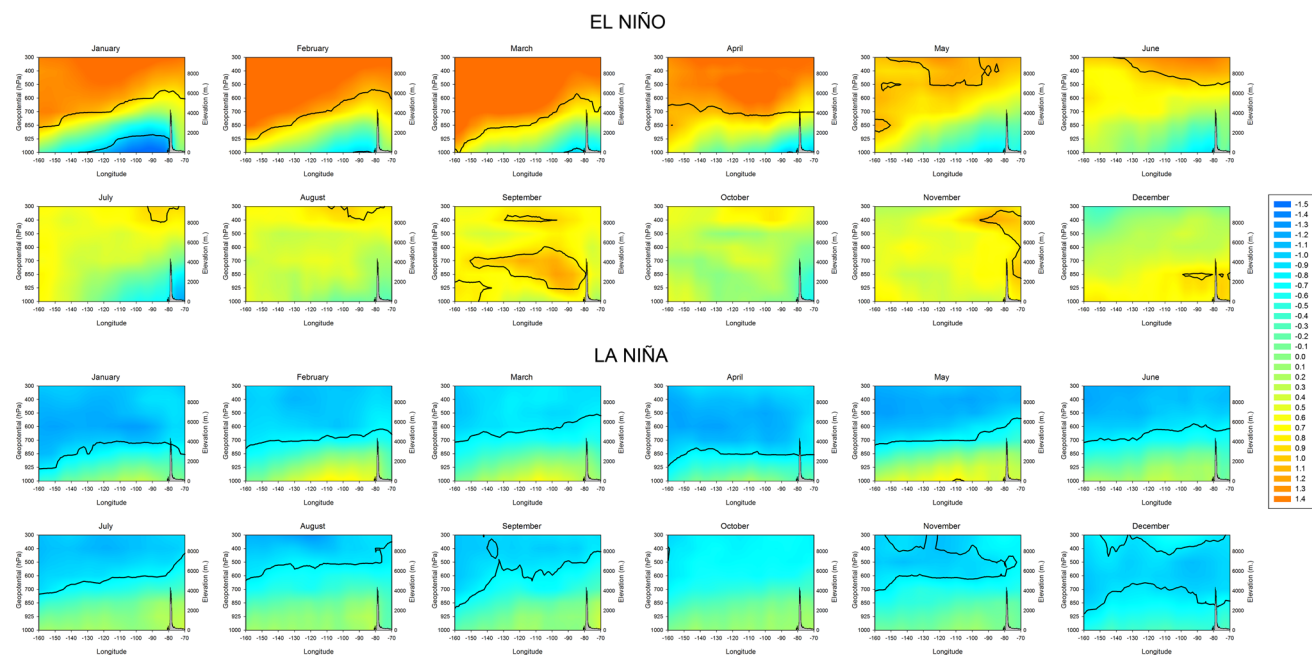


**Fig. 13** Monthly geopotential height anomalies corresponding to El Niño and La Niña phases from El Niño 1 + 2 Index in a profile between  $-160^{\circ}\text{E}$  and  $-70^{\circ}\text{E}$  at  $-1^{\circ}\text{S}$ . Black line isolates heights and

regions in which the geopotential anomalies are significantly different to the rest of the years

those showed for El Niño 3.4 would also help to explain the strong asymmetric response of the SPEI in this region to these phases, since the warm phases produce stronger SLP and geopotential anomalies than the cold phases.

The different physical mechanisms and propagation of El Niño effects in the two regions is evident when analyzing the influence of the vertical velocity ( $\omega$ ) on the SPEI in the two regions. Figure 14 shows the correlation of the monthly 1-month SPEI for Varimax Pattern 1 (Andes) and 2 (Western plains) with  $\omega$  values at different geopotential levels in the same geographic profile. The main conclusion is the negative correlation with  $\omega$  over the Andes and over the western plains. Nevertheless, there are strong differences in the correlation between the monthly 1-month SPEI and the vertical velocity between the two regions. For the Andean region, the correlation pattern shown is compatible with the Walker circulation; there are clear differences between the central Pacific region (showing positive correlations in some months of the year -January, February, June-) and the eastern Pacific close to the Andes in which negative correlations are also found in March, April, May, June and December. Nevertheless, correlations are not strong and only affecting few regions and levels. On the contrary, the Western plains show a clear pattern characterized by strong negative correlations between the monthly 1-month SPEI and monthly  $\omega$  values. The negative correlation means that strong and negative  $\omega$  levels are associated with convective processes and

ascending (descending) of air causes humid (dry) conditions in the Western plains. This pattern is observed for most months, but a higher intensity is recorded from March to June, coinciding with the months in which strong correlations between SPEI and SST in the eastern Pacific region are found. The effect of the relief is evident given that areas with negative and significant correlations between the SPEI in the Western plains and  $\omega$  are mainly restricted to the west of the Andes.

This distinct pattern in the influence of the vertical velocity on the SPEI of the Andes and Western plains values is driven by the different behavior observed during El Niño 1 + 2 warm phases. Thus, during El Niño 3.4 warm and cold phases there are no significant anomalies in the vertical velocity at different geopotential levels in the region of Ecuador, and the influence is restricted to the central Pacific between January and March (Fig. 15). The anomalies in vertical velocity are much more evident during El Niño 1 + 2 warm phases (Fig. 16). El Niño events show negative  $\omega$  anomalies, characterized by above of the normal air ascending velocity in a large region of the central Pacific but also showing significant above of the normal values at different geopotential levels in the Western plains between January and July. On the contrary, during the La Niña episodes there are dominant positive anomalies in the vertical velocity, that although characterized by dominant descending air in the Western plains region, they show much lower intensity than that showed

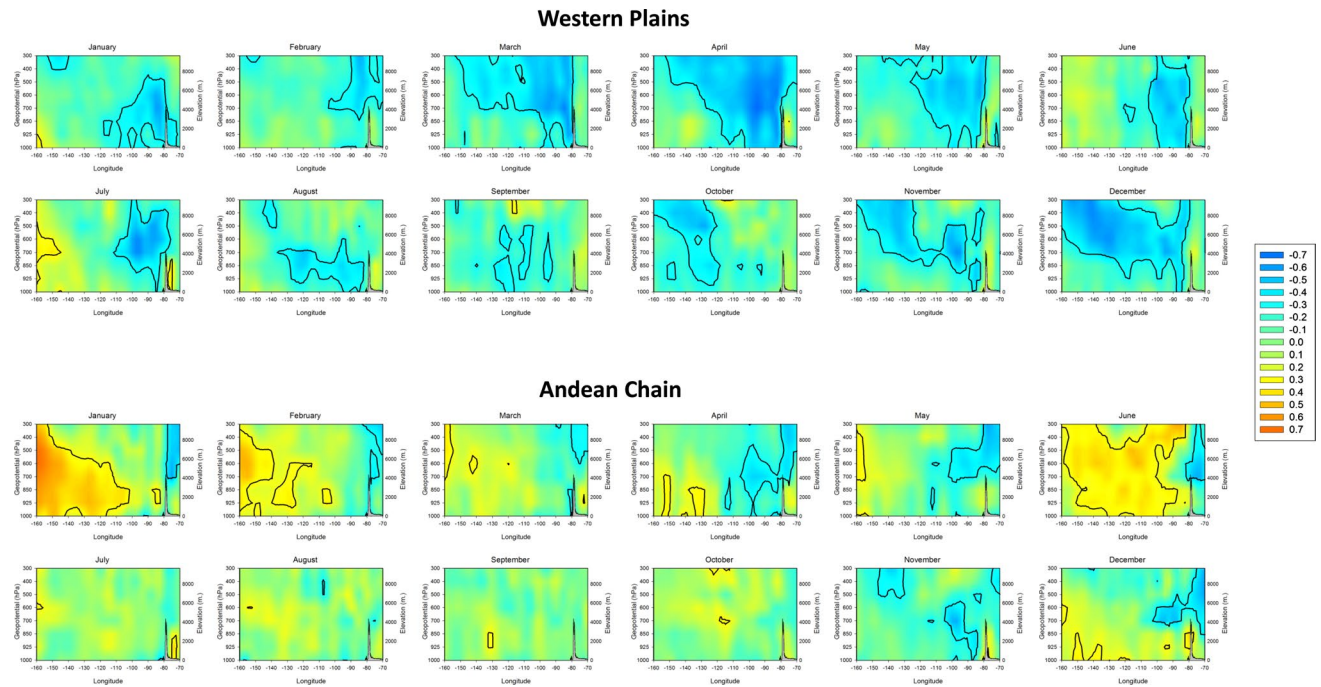


**Fig. 14** Monthly correlation between 1-month SPEI corresponding to the evolution of Varimax Pattern 1 (Andean Chain) and Varimax Pattern 2 (Western Plains) and vertical velocity ( $\omega$ ) at different heights in a profile between  $-160^{\circ}\text{E}$  and  $-70^{\circ}\text{E}$  at  $-1^{\circ}\text{S}$ . *Black lines*

isolate regions and levels with significant correlations. The topography of the Andean chain is represented for facilitating the interpretation

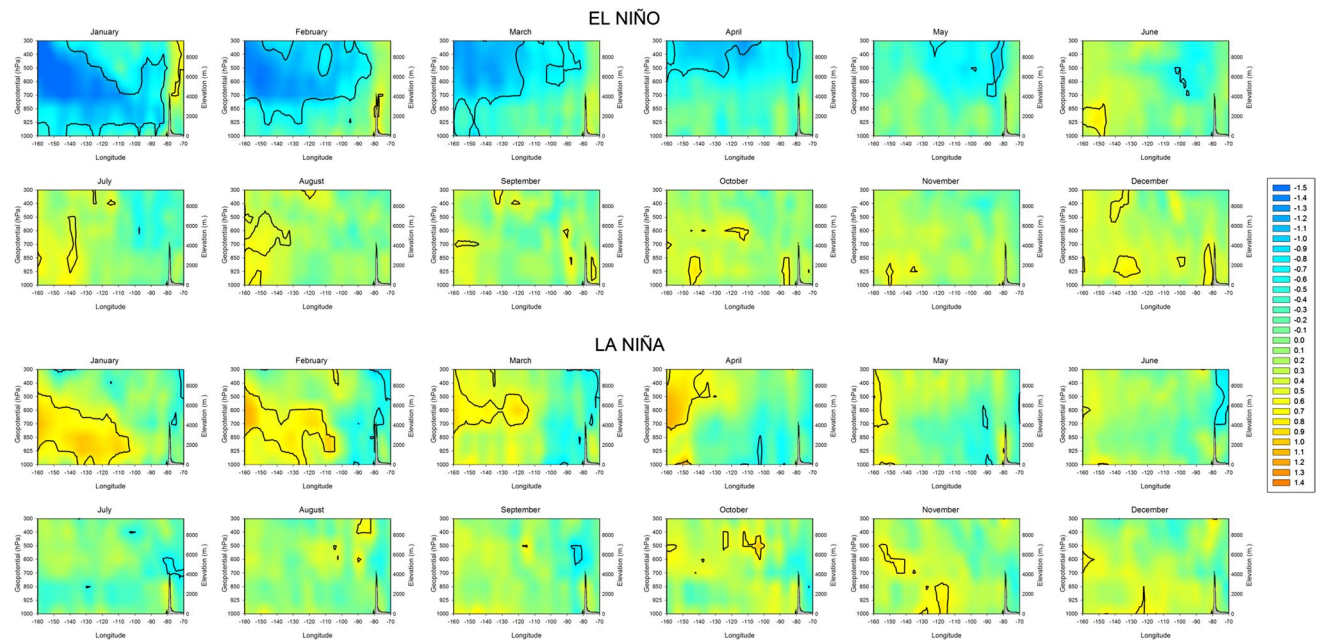


**Fig. 15** Monthly vertical velocity anomalies ( $\omega$ ) anomalies corresponding to El Niño and La Niña phases from the El Niño 3.4 Index in a profile between  $-160^{\circ}\text{E}$  and  $-70^{\circ}\text{E}$  at  $-1^{\circ}\text{S}$ . *Black line* isolates

heights and regions in which the geopotential anomalies are significantly different to the rest of the years

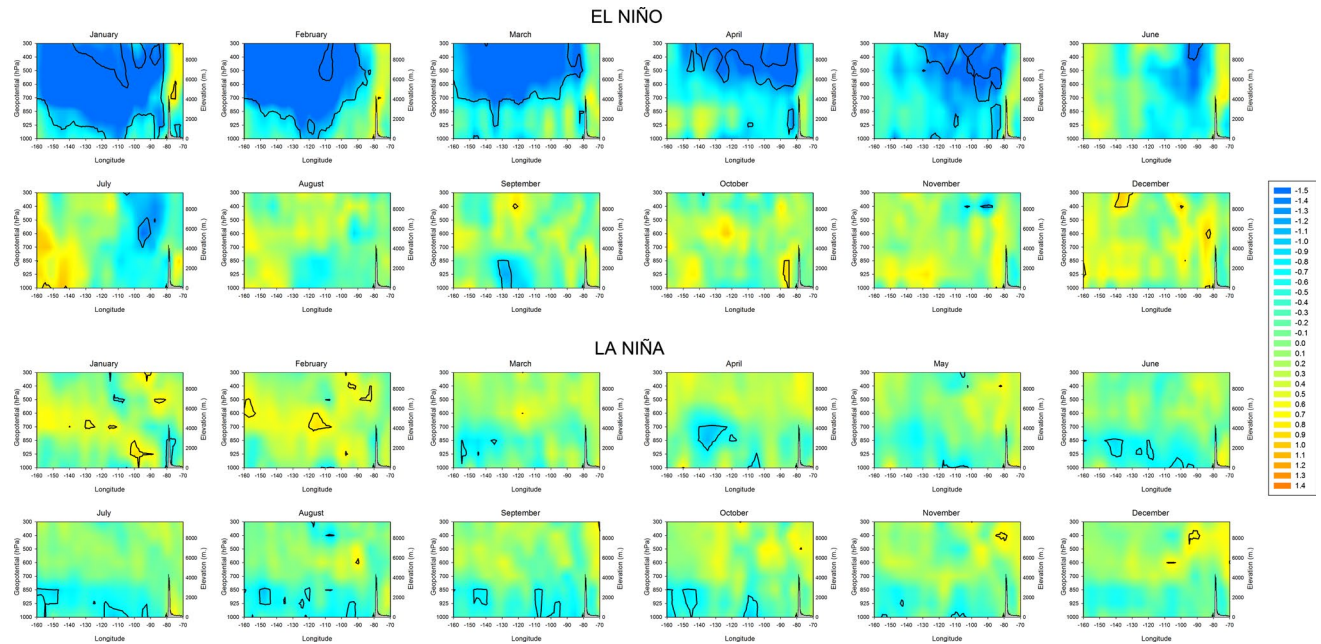


**Fig. 16** Monthly vertical velocity anomalies ( $\omega$ ) anomalies corresponding to El Niño and La Niña phases from El Niño 1 + 2 Index in a profile between  $-160^{\circ}\text{E}$  and  $-70^{\circ}\text{E}$  at  $-1^{\circ}\text{S}$ . *Black line* isolates

heights and regions in which the geopotential anomalies are significantly different to the rest of the years

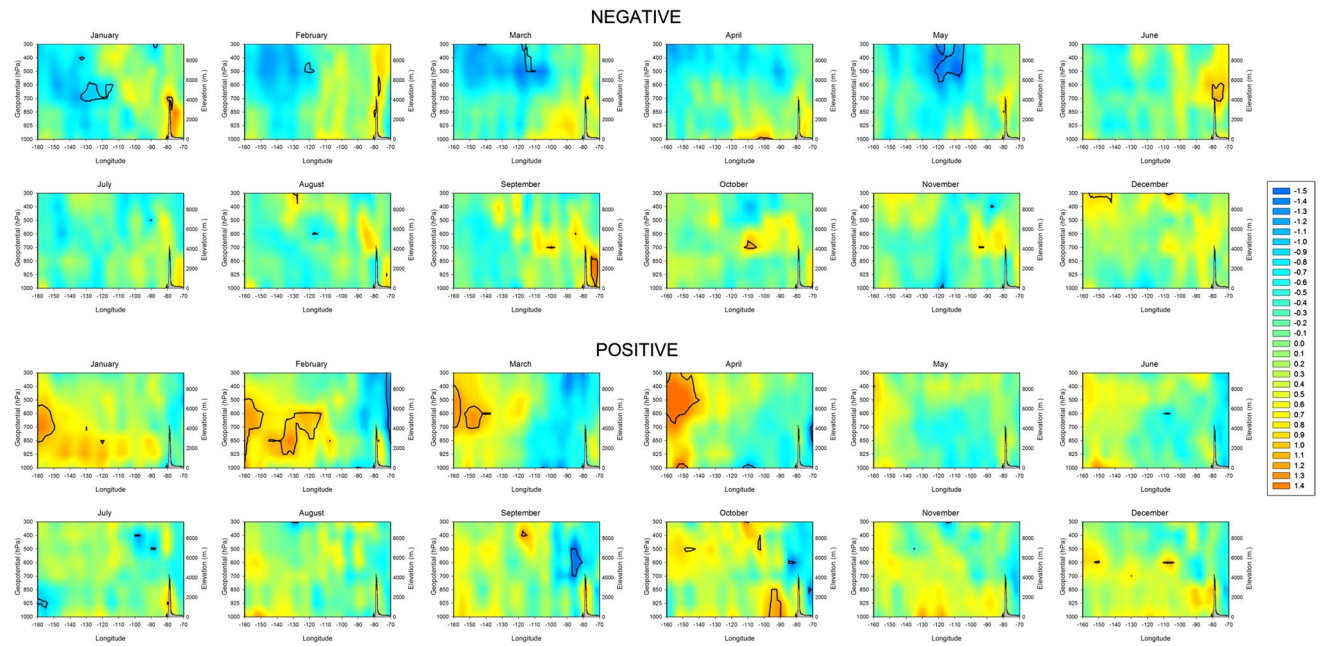


**Fig. 17** Monthly vertical velocity anomalies ( $\omega$ ) corresponding to the three most humid (1974, 1999, 2008) and dry (1985, 1987, 1992) years in the Andean region (Varimax Pattern 1) in a profile

between  $-160^{\circ}\text{E}$  and  $-70^{\circ}\text{E}$  at  $-1^{\circ}\text{S}$ . *Black line* isolates heights and regions in which  $\omega$  anomalies are significantly different to the rest of the years

for El Niño phases. Thus, whereas these configurations do not show any agreement with the vertical velocity anomalies during the driest and most humid years recorded in the

Andes region (Fig. 17), there is a strong agreement with the vertical velocity anomalies in the dry and humid years recorded in the Western plains, characterized by dominant

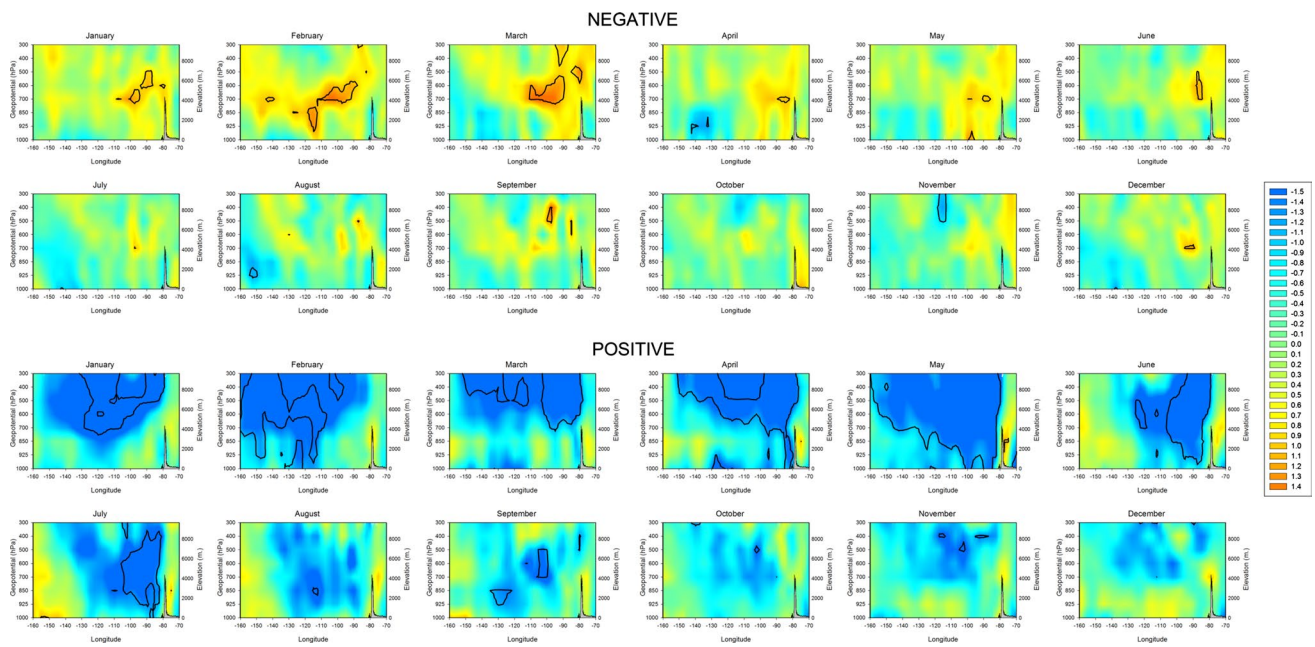


**Fig. 18** Monthly vertical velocity anomalies ( $\omega$ ) corresponding to the three most humid (1983, 1997, 1998) and dry (1968, 1985, 1990) years in the Western plains region (Varimax Pattern 2) in a pro-

file between  $-160^{\circ}\text{E}$  and  $-70^{\circ}\text{E}$  at  $-1^{\circ}\text{S}$ . *Black line* isolates heights and regions in which  $\omega$  anomalies are significantly different to the rest of the years

descending and ascending air anomalies, respectively over the Western plain region (Fig. 18).

## 4 Discussion

### 4.1 Drought spatial variability

We showed the spatial variability of droughts in Ecuador, finding two main regions that are controlled by the spatial diversity of topography: the Andean chain that crosses the mid of the country with a North–South direction, with average elevations above 4000 m.a.s.l and peaks of 6300 m, and the Western plains, covering a 200 km distance between the Pacific ocean and the Andes. These two regions showed high spatial homogeneity in terms of the temporal evolution of droughts, with very few differences between the meteorological stations located in each region. Climate information is scarce in the eastern part of the country (Amazonia) and it is not possible to attribute a distinct evolution of droughts over this region. These drought patterns coincide with the general climate regionalization of Ecuador based on precipitation and air temperature data. Recently, Morán-Tejeda et al. (2015) have shown that precipitation in Ecuador exhibits the same spatial patterns shown here for droughts. These authors showed a more complex temporal pattern for air temperature than for precipitation, as a consequence of differences in the Andes sector, in which

some meteorological stations show a clear air temperature increase whereas others show no relevant changes during the recent decades. Therefore, although droughts have been quantified here considering both, the precipitation and the atmospheric evaporative demand, the temporal variability of the droughts seems to mostly depend on the precipitation variability across the country, in agreement with a recent study by Vicente-Serrano et al. (2015), that showed that droughts are mainly controlled by changes in the atmospheric evaporative demand in dry areas, but determined by precipitation variability in humid regions, such as Ecuador.

Temporal evolution showed a trend toward lower drought conditions in the Western plains, in agreement with the significant precipitation increase found in this region (Moran-Tejeda et al. 2015) and although atmospheric evaporative demand has probably increased as a consequence of the air temperature rise, its effect on drought severity is hidden by the strong precipitation increase. On the contrary, in the Andes, severe drought episodes have been identified since 2000, and probably atmospheric evaporative demand is having a negative role in the severity of these events.

### 4.2 General drought mechanisms

This study found that the differences in the drought evolution between the Andean chain and Western plains are mainly related to the complex influence of ENSO. We have found that the sign of correlations between the SPEI and ENSO in

the two studied regions is the same no matter which ENSO index (i.e., El Niño 3.4 and El Niño 1 + 2) is considered: negative in the Andean chain and positive in the Western plains. Nevertheless, we have found highest correlation between the SPEI variability and the El Niño 3.4 Index in the Andes, whereas in the Western plains there are highest correlations with the El Niño 1 + 2 index. Different studies had observed that two types of El Niño (canonical, characterized by an eastern displacement of the SST anomalies, and Modoki, characterized by a central Pacific SST anomalies) lead to different impacts on climate variability from regional to global scale via the atmospheric teleconnection (Cai and Cowan 2009; Yoon et al. 2012; Yeh et al. 2014). Here we reported clear differences in the sensitivity of droughts to SST anomalies in the central and eastern Pacific regions. Thus, in the Andes, the occurrence of droughts is clearly linked to the central El Niño phases (identified by means of El Niño 3.4 index), whereas in the Western plains the central El Niño phases do not cause droughts but humid conditions. On the contrary, the ENSO phases identified with El Niño 1 + 2 index do not cause SPEI anomalies in the Andes, but they are clearly related to very dry and very humid conditions in the Western plains for the cold and warm phases, respectively. Therefore, this pattern can be seen in areas separated only by 200 km of horizontal distance, but by more than 4000 m in the vertical. Accordingly, the results show that very different ENSO flavors seems to drive drought variability in a small country like Ecuador.

#### 4.2.1 Drought mechanisms in the Andes of Ecuador

The effects of the central ENSO are propagated thousands of kilometers to the Andes region by the mid-troposphere. In a study of the effect of ENSO on droughts worldwide, Vicente-Serrano et al. (2011a, b) showed that high (low) pressure SLP anomalies in the central Pacific region between September of the previous year to April of El Niño (La Niña) year propagates to the mid-level troposphere between November of the previous year to June of El Niño year (particularly stronger in February–March), determining the occurrence of strong high (low) pressure anomalies at the 500 hPa level in most of the intertropical area, including Ecuador. We showed that the warm SST anomalies in central Pacific promote convection in this region (decreasing SLP and increasing the ascending vertical velocity), but the propagation in the intertropical region reinforces anti-cyclonic conditions at mid-level of the troposphere. The opposite pattern is found during La Niña phases, which are prone to cause humid conditions in the Andes of Ecuador. Different studies had stressed the change in the Walker circulation associated with ENSO as the main driver of drought variability in the northern Andean region (e.g., Kousky et al. 1984; Francou et al. 2004; Vuille 1999; Vuille

et al. 2000b; Poveda et al. 2006, 2011). El Niño events have been proven to reveal clear westerly wind anomalies in the central Pacific region, while La Niña is generally associated with easterly wind anomalies in the lower troposphere and the reverse flow in the higher troposphere (Wang 2002). We found that this pattern is more persistent in some months of the year (mainly during the boreal winter and summer), coinciding with the humid and dry seasons in Ecuador, but if the pattern is sustained during some months of the year the drought conditions may propagate throughout several months and drought time-scales.

During La Niña years there is an increase of convective processes over the entire Amazon basin, and an enhancement of the easterly flow and associated Amazonian moisture transport during the wet season, which is extended westward over the tropical and subtropical Andes (Kousky and Kayano 1994; Vuille 1999; Francou et al. 2004), which would favor humid conditions in this region. In this case drought would be suppressed by above normal precipitation, but also by greater cloud cover, which means lower incoming radiation, and lower air temperatures in the central Andes, which would reduce the atmospheric evaporative demand (AED).

We would like to stress that to explain the influence of all these physical mechanisms associated with warm and cold SST conditions in the central Pacific region, the Andean relief plays a determining role given a high elevation that interacts with circulation processes in the mid-troposphere region and reduces the effect of eastern Pacific deep convection (Xu et al. 2004). Thus, the negative correlation between drought severity and the SST anomalies in the central Pacific region would explain the strong sensitivity of glaciers in the Andes of Ecuador to central Pacific El Niño and La Niña events (Francou et al. 2004; Vuille et al. 2008).

#### 4.2.2 Drought mechanisms in the Western plains

The response of droughts in the Western plains of Ecuador to warm and cold SST anomalies in the Pacific shows a very different pattern to that observed in the Andes. In this case, the effect of the eastern Pacific SST anomalies is directly related to an enhancement (decrease) of the convective activity corresponding to warm (cold) phases. Some studies have discussed the significant changes in precipitation, cloud cover, and air temperature that occur during ENSO all along the Pacific coast and the western slope of the Ecuadorian Andes (Rossel et al. 1999; Bendix 2000; Vuille et al. 2000b; Bendix et al. 2011). Here we showed that these changes are mainly driven by the enhanced (suppressed) tropical convection as a response to warm (cold) SST in the eastern Pacific. This is clearly illustrated by the strong vertical velocity (omega) air ascending anomalies in this region corresponding to warm SST in the eastern

Pacific, with associated thunderstorms, which are restricted to the Plains close to the Pacific Ocean and the western slopes of the Andes. Therefore, warm SST anomalies in the eastern Pacific drive an intensification of the meridional overturning tropical circulation (the regional Hadley circulation), with more vigorous vertical ascent, favorable for the convective activity observed during the warm phases. This pattern is accompanied by westerly wind anomalies that bring moisture from a warm ocean and trigger strong floods in the region (Bendix et al. 2011). We found that these conditions are persistent for different months of the year, even at short time-scales (significant SPEI anomalies are identified at 1-month time-scales from October of the previous year to June of El Niño year), coinciding with the humid season, but the anomalies propagate further months after throughout longer SPEI time-scales.

Bendix et al. (2011) analyzed the response of precipitation variability to some ENSO events in a region of the southern Ecuador Plains, and stressed that SST conditions in the eastern Pacific can prevail even if the central Pacific exhibits the opposite phases (e.g., warm conditions in the East and cold conditions in the central Pacific as observed in 2008), demonstrating that central Pacific SST are becoming more unreliable indicators for drought and flood situation in the southwestern areas of Ecuador. Results reveal that this pattern can be generalized to the whole Western plains of Ecuador, in which cold SST in the eastern Pacific is highly prone to cause drought in this region as a consequence of dominant easterly winds and descending air in the area. We also indicated that droughts have been less frequent in the past two decades in this region, which is clearly linked to the low frequency of eastern La Niña episodes. Studies have shown that the regional Hadley circulation has indeed intensified in the past decades, with more vigorous ascents in the tropics between  $\sim 10^{\circ}\text{S}$  and  $10^{\circ}\text{N}$  (Vuille et al. 2008). This would explain the increase of annual precipitation observed (Morán-Tejeda et al. 2015) and the higher magnitude and duration of humid periods observed with the SPEI series.

### 4.3 Non-symmetric patterns

In this work, results showed that droughts in Ecuador do not respond linearly to both El Niño and La Niña phases. Thus, the strong asymmetry has been found in the response to the warm and cold phases, both in the Andes and Western plains as a response to the central Pacific and eastern Pacific SST anomalies, respectively. This pattern is characteristic of the drought response to El Niño and La Niña phases at the global scale (Vicente-Serrano et al. 2011a, b). In the Andes, we found that the response to the central Pacific La Niña phases (prone to moist conditions) is recorded earlier and it is stronger and more persistent than

the response to El Niño phases (prone to dry conditions). The pattern is the opposite in the Western plains, with a stronger response to the eastern Pacific El Niño (humid conditions) than La Niña events (dry conditions). In both regions the response is higher corresponding to the episodes prone to cause high precipitation. Different studies found that the asymmetric component is indeed a fundamental property of atmospheric responses to recent ENSO forcing (e.g., Frauen et al. 2014; Zhang et al. 2014; Chen et al. 2015). This is explained by the strong asymmetric circulation mechanisms observed during El Niño and La Niña phases in both central and eastern ENSO configurations.

The central Pacific La Niña phases show more persistent mid- and upper-troposphere geopotential anomalies than El Niño phases in the Eastern Pacific region. This would favor that La Niña events are more prone to cause humid conditions in the Andes than El Niño cause dry conditions. The opposite is found for the eastern Pacific cold and warm phases. The eastern El Niño phases show very strong SLP (negative) and geopotential at high levels (positive) anomalies much more pronounced than the counterpart anomalies observed during La Niña phases. In addition, convection enhancement (suppression) during warm (cold) phases shows strong nonlinear patterns in the eastern Pacific since vertical ascending air velocity is very strong during El Niño phases, but descending vertical air during cold phases is not characterized by strong anomalies. This agrees with recent results by Frauen et al. (2014), which showed that the ENSO events in the East Pacific show stronger nonlinearities than Central Pacific events.

The physical mechanisms that cause non-linear pattern in both regions are not well understood. Hoerling et al. (1997) indicated that the interpretation of this behavior is complicated, but they noted that composite warm event SST anomalies are not the exact inverse of their cold event counterparts. Meinen and McPhaden (2000) showed that the volume of warm water in the equatorial Pacific Ocean is related to the magnitude of the ENSO anomalies since for a given change in equatorial warm water volume, the corresponding warm El Niño SST anomalies are larger than the corresponding cold La Niña anomalies. The asymmetry of the spatial propagation between El Niño and La Niña events could explain this behavior, since specifically, El Niño anomalies tend to propagate eastward and La Niña anomalies westward (McPhaden and Zhang 2009).

The important role of differences in the spatial pattern during El Niño and La Niña phases has been also stressed by Dommenges et al. (2013) who showed that central Pacific events tend to be weak El Niño or strong La Niña events. In turn, east Pacific events tend to be strong El Niño or weak La Niña events. These authors also showed that the zonal wind response to SST anomalies during strong El Niño events is stronger and shifted to the east relative

to strong La Niña events, supporting the eastward shifted El Niño pattern and the asymmetric time evolution. This would agree with the different ENSO zones that trigger high precipitation conditions in the Andes and the Western plains of Ecuador.

## 5 Concluding remarks

Here we have analyzed drought variability in Ecuador and identified a complex ENSO influence on the occurrence of drought episodes in the region. The main conclusions of this study are:

- Two patterns of drought evolution have been found in Ecuador, corresponding to the Andes and the Western plains. Drought has showed a trend toward less severe and frequent in the Western plains, but no changes in drought severity are observed in the Andes.
- Sea Surface Temperature (SST) anomalies in the central and eastern Pacific regions have very different influence in the Andes and Western plains. El Niño 3.4 index, characteristic of the central Pacific region, is related to drought variability in the Andes. El Niño 1 + 2 index, which informs of SST anomalies in the eastern Pacific, is controlling drought variability in the Western plains.
- El Niño phases in the central Pacific region are propagated throughout the mid-troposphere, causing upper level high pressures and drought conditions in the Andes region, which are sustained during different months of the year and propagated throughout long drought time-scales.
- La Niña phases in the eastern Pacific causes droughts in the Western plains throughout the suppression of westerly flows and convective processes.
- There is a strong nonlinear response of the Andes and Western plains to warm and cold phases in the central and eastern Pacific, respectively. The ENSO phases that produce humid conditions in both regions cause stronger anomalies in the drought index than the counterpart phase.

We would like to stress that other atmospheric circulation mechanisms, in addition to ENSO, may contribute to the development of droughts in Ecuador, e.g. the Pacific Decadal Oscillation (Poveda et al. 2002) or other regional and local atmospheric processes (Poveda et al. 2006; Bendix et al. 2011). Here, we focus on the complex impact of the ENSO in the entire country, and showed the strong importance of this coupled ocean atmospheric processes to explain drought variability in the region. We have stressed the need of considering different indices linked to different SST spatial configurations in the Pacific region to predict and monitor droughts in the entire country. For this reason, current ENSO

projections that focus on the severity of El Niño and La Niña events, but also on the spatial configurations of the ENSO phases are strongly relevant. Thus, recently Cai et al. (2014, 2015) have stressed possible reinforcement of both eastern and central ENSO warm and cold phases in the future, which could favor the frequency and severity of climate extremes in the different regions of Ecuador.

**Acknowledgments** This work was supported by the EPhysLab (UVIGO-CSIC Associated Unit) and the research projects I-COOP H2O 2013CD0006: “Test multisectorial y actividades demostrativa sobre el potencial desarrollo de sistemas de monitorización de sequías en tiempo real en la región del oeste de Sudamérica” financed by the Spanish National Research Council, CGL2011-27574-CO2-02, CGL2014-52135-C03-01 and Red de variabilidad y cambio climático RECLIM (CGL2014-517221-REDT), financed by the Spanish Commission of Science and Technology and FEDER, and “LIFE12 ENV/ES/000536-Demonstration and validation of innovative methodology for regional climate change adaptation in the Mediterranean area (LIFE MEDACC)” financed by the LIFE programme of the European Commission. Cesar Azorin-Molina was supported by the JCI-2011-10263 Grant. Arturo Sanchez-Lorenzo was supported by the JCI-2012-12508 Grant. Miquel Tomas-Burguera was supported by a doctoral grant by the Ministry of Economy and Competitiveness and Natalia Martin-Hernandez was supported by a doctoral grant by the Aragón Regional Government. E. Aguilar was funded by the Grant CCI-009-ATN/OC-12439-RG-2012 from the Banco Iberoamericano de Desarrollo.

## References

- Ashok K, Behera SK, Rao SA, Weng H, Yamagata T (2007) El Niño Modoki and its possible teleconnection. *J Geophys Res Atmos* 112:C11007. doi:10.1029/2006JC003798
- Barry RG, Carleton AM (2001) *Synoptic and dynamic climatology*. Routledge, London
- Beguéría S, Vicente-Serrano SM, Reig F, Latorre B (2014) Standardized Precipitation Evapotranspiration Index (SPEI) revisited: parameter fitting, evapotranspiration models, kernel weighting, tools, datasets and drought monitoring. *Int J Climatol* 34:3001–3023
- Bendix J (2000) Precipitation dynamics in Ecuador and northern Peru during the 1991/92 El Niño: a remote sensing perspective. *Int J Remote Sens* 21:533–548
- Bendix J, Lauer W (1992) Die Niederschlagsjahreszeiten in Ecuador und ihre klimadynamische interpretation. *Erdkunde* 46:118–134
- Bendix J, Trachte K, Palacios E, Rollenbeck R, Göttlicher D, Nauss T, Bendix A (2011) El Niño meets La Niña-anomalous rainfall patterns in the “traditional” El Niño region of Southern Ecuador. *Erkunde* 65:151–167
- Borlace S, Cai W, Santos A (2013) Multidecadal ENSO amplitude variability in a 1000-yr simulation of a coupled global climate model: Implications for observed ENSO variability. *J Clim* 26:9399–9407
- Bourma MJ, Dye C (1997) Cycles of malaria associated with El Niño in Venezuela. *J Am Med Assoc* 3:1772–1774
- Buytaert W, Celleri R, Willems P, Bièvre BD, Wyseure G (2006) Spatial and temporal rainfall variability in mountainous areas: a case study from the south Ecuadorian Andes. *J Hydrol* 329:413–421
- Cai W, Cowan T (2009) La Niña Modoki impacts Australia autumn rainfall variability. *Geophys Res Lett* 36:L12805. doi:10.1029/2009-GL037885

- Cai W et al (2014) Increasing frequency of extreme El Niño events due to greenhouse warming. *Nat Clim Change* 4:111–116
- Cai W et al (2015) Increased frequency of extreme La Niña events under greenhouse warming. *Nat Clim Change* 5:132–137
- Caussinus H, Mestre O (2004) Detection and correction of artificial shifts in climate series. *J R Stat Soc Ser C* 53(3):405–425. doi:[10.1111/j.1467-9876.2004.05155.x](https://doi.org/10.1111/j.1467-9876.2004.05155.x)
- Celleri R, Willems P, Buytaert W, Feyen J (2007) Space-time rainfall variability in the Paute basin, Ecuadorian Andes. *Hydrol Process* 21:3316–3327
- Changnon SA, Easterling WE (1989) Measuring drought impacts: the Illinois case. *Water Resour Bull* 25:27–42
- Chen D et al (2015) Strong influence of westerly wind bursts on El Niño diversity. *Nat Geosci* 8:339–345
- Córdoba-Machado S, Palomino-Lemus R, Gámiz-Fortis S, Castro-Díez Y, Esteban-Parra MJ (2015) Assessing the impact of El Niño Modoki on seasonal precipitation in Colombia. *Glob Planet Change* 124:241–261
- Dai A (2011) Drought under global warming: a review. *Wiley Interdiscip Rev Clim Change* 2:45–65
- Dai A (2013) Increasing drought under global warming in observations and models. *Nat Clim Change* 3:52–58
- Dewitte B, Vazquez-Cuervo J, Goubanova K, Illig S, Takahashi K, Cambon G, Purca S, Correa D, Gutierrez D, Sifeddine A, Ortlieb L (2012) Change in El Niño flavours over 1958–2008: implications for the long-term trend of the upwelling off Peru. *Deep Sea Res Part II* 77–80:143–156
- Dommenget D, Bayr T, Frauen C (2013) Analysis of the non-linearity in the pattern and time evolution of El Niño southern oscillation. *Clim Dyn* 40:2825–2847
- Droogers P, Allen RG (2002) Estimating reference evapotranspiration under inaccurate data conditions. *Irrigat Drain Syst* 16:33–45
- Drumond A, Ambrizzi T (2006) Inter ENSO variability and its influences over the South American Monsoon System. *Adv Geosci* 6:167–171
- Francou B, Vuille M, Favier V, Cáceres B (2004) New evidence for an ENSO impact on low-latitude glaciers: Antizana, Andes of Ecuador. *J Geophys Res* 109:D18106. doi:[10.1029/2003JD004484](https://doi.org/10.1029/2003JD004484)
- Frauen C, Dommenget D, Tyrrell N, Rezny M, Wales S (2014) Analysis of the nonlinearity of El Niño-Southern Oscillation Teleconnections. *J Clim* 27:6225–6244
- Gagnon AS, Smoyer-Tomic KE, Bush ABG (2002) The El Niño southern oscillation and malaria epidemics in South America. *J Biometeorol* 46:81–89
- Hamilton SK, Sippel SJ, Melack JM (2002) Comparison of inundation patterns among major South American floodplains. *J Geophys Res*. doi:[10.1029/2000JD000306](https://doi.org/10.1029/2000JD000306)
- Hamilton SK, Sippel SJ, Melack JM (2004) Seasonal inundation patterns in two large savanna floodplains of South America: the Llanos de Moxos (Bolivia) and the Llanos del Orinoco (Venezuela and Colombia). *Hydrol Process* 18:2103–2116
- Hargreaves GL, Allen RG (2003) History and evaluation of Hargreaves evapotranspiration equation. *J Irrig Drain Eng ASCE* 129:53–63
- Hargreaves GL, Samani ZA (1985) Reference crop evapotranspiration from temperature. *Appl Eng Agric* 1:96–99
- Haylock MR, Peterson TC, Alves LM et al (2006) Trends in total and extreme South American rainfall in 1960–2000 and links with sea surface temperature. *J Clim* 19:1490–1512
- Hoerling MP, Kumar A, Zhong M (1997) El Niño, La Niña, and the nonlinearity of Their teleconnections. *J Clim* 10:1786–1789
- Huth R (2006) The effect of various methodological options on the detection of leading modes of sea level pressure variability. *Tellus Ser A* 58:121–130
- Jiménez-Muñoz JC, Sobrino JA, Mattar C, Malhi Y (2013) Spatial and temporal patterns of the recent warming of the Amazon forest. *J Geophys Res Atmos* 118:5204–5215
- Johnson NC (2013) How many ENSO flavors can we distinguish? *J Clim* 26:4816–4827
- Jolliffe IT (1986) *Principal component analysis*. Springer, New York
- Jolliffe IT (1990) *Principal component analysis: a beginner's guide*. Part I: Introduction and application. *Weather* 45:375–382
- Kalnay E (1996) The NCEP/NCAR 40-year reanalysis project. *Bull Am Meteorol Soc* 77:437–471
- Kousky VE, Kayano MT (1994) Principal modes of outgoing long-wave radiation and 250-mb circulation for the South American sector. *J Clim* 7:1131–1143
- Kousky VE, Kayano MT, Cavalcanti IFA (1984) A review of the Southern Oscillation: oceanic-atmospheric circulation changes and related rainfall anomalies. *Tellus Ser A* 36 A:490–504
- Künzler M, Huggel C, Ramírez JM (2012) A risk analysis for floods and lahars: case study in the Cordillera Central of Colombia. *Nat Hazards* 64:767–796
- Lee T, McPhaden M (2010) Increasing intensity of El Niño in the central-equatorial Pacific. *Geophys Res Lett* 37:L14603. doi:[10.1029/2010GL044007](https://doi.org/10.1029/2010GL044007)
- Lewis SL, Brando PM, Phillips OL, Van Der Heijden GMF, Nepstad D (2011) The 2010 Amazon drought. *Science* 331:554
- Li G, Li Ch, Tan Y, Pan J (2013) Impacts of the central and eastern Pacific types of ENSO on sea surface temperature in the South Pacific. *Theor Appl Climatol* 114:315–327
- Lyon B (2003) Enhanced seasonal rainfall in Northern Venezuela and the extreme events of December 1999. *Hydrol Process* 18:2103–2116
- Marengo JA, Nobre CA, Tomasella J et al (2008) The drought of Amazonia in 2005. *J Clim* 21:495–516
- McKee TB, Doesken NJ, Kleist J (1993) The relationship of drought frequency and duration to time scales. In: Paper presented at 8th conference on applied climatology (Anaheim, CA: Am. Meteorol. Soc.)
- McPhaden MJ, Zhang X (2009) Asymmetry in zonal phase propagation of ENSO sea surface temperature anomalies. *Geophys Res Lett*. doi:[10.1029/2009GL038774](https://doi.org/10.1029/2009GL038774)
- McVicar TR et al (2012) Global review and synthesis of trends in observed terrestrial near surface wind speeds: implications for evaporation. *J Hydrol* 416(417):182–205
- Meinen Ch, McPhaden J (2000) Observations of warm water volume changes in the equatorial Pacific and their relationship to El Niño and La Niña. *J Clim* 13:3551–3559
- Mestas-Núñez A (2000) Orthogonally properties of rotated empirical modes. *Int J Climatol* 20:1509–1516
- Mestre O, Domonkos P, Picard F, Auer I, Robin S, Lebarbier E, Böhm R, Aguilar E, Guijarro J, Vertacnik G, Klančar M, Dubuisson B, Stepanek P (2013) HOMER: HOMogenisation softwarE in R- methods and applications. *Időjárás* 117:47–67
- Mo KC, Berbery EH (2011) Drought and persistent wet spells over South America based on observations and the U.S. CLIVAR drought experiments. *J Clim* 16:2302–2306
- Moran-Tejeda E et al (2015) Climate trends and variability in Ecuador (1966–2011). *Int J Climatol*. doi:[10.1002/joc.4597/abstract](https://doi.org/10.1002/joc.4597/abstract)
- Mosquera-Machado S, Ahmad S (2007) Flood hazard assessment of Atrato River in Colombia. *Water Resour Manag* 21:591–609
- Olivares I, Svenning J-C, van Bodegom PM, Balslev H (2015) Effects of warming and drought on the vegetation and plant diversity in the Amazon Basin. *Bot Rev* 81:42–69
- Paredes FJ, Guevara E (2013) A probabilistic model for the prediction of meteorological droughts in Venezuela. *Atmosfera* 26:311–323
- Penman HL (1948) Natural evaporation from open water, bare soil, and grass. *Proc R Soc Lond A* 193:120–146
- Phillips OL et al (2009) Drought sensitivity of the amazon rainforest. *Science* 323:1344–1347

- Picard F, Lebarbier E, Hoebcke M, Rigail G, Thiam B, Robin S (2011) Joint segmentation calling and normalization of multiple CGH profiles. *Biostatistics* 12:413–428
- Poveda G, Mesa OJ (1997) Feedbacks between hydrological processes in tropical South America and large-scale ocean-atmospheric phenomena. *J Clim* 10:2690–2702
- Poveda G et al (2002) Influencia de fenómenos macro climáticos sobre el ciclo anual de la hidrología colombiana: cuantificación lineal, no lineal y percentiles probabilísticos. *Meteorol Colomb* 6:121–130
- Poveda G, Waylen PR, Pulwarty RS (2006) Annual and inter-annual variability of the present climate in northern South America and southern Mesoamerica. *Palaeogeogr Palaeoclimatol Palaeoecol* 234:3–27
- Poveda G, Álvarez D, Rueda Ó (2011) Hydro-climatic variability over the Andes of Colombia associated with ENSO: a review of climatic processes and their impact on one of the Earth's most important biodiversity hotspots. *Clim Dyn* 36:2233–2249
- Rayner NA et al (2003) Global analyses of sea surface temperature, sea ice, and night marine air temperature since the late nineteenth century. *J Geophys Res D Atmos* 108:ACL 2-1–ACL 2-29
- Richman MB (1986) Rotation of principal components. *J Climatol* 6:293–335
- Rollenbeck R, Bendix J (2011) Rainfall distribution in the Andes of southern Ecuador derived from blending weather radar data and meteorological field observations. *Atmos Res* 99:277–289
- Rollenbeck R, Bendix J, Fabian P (2011) Spatial and temporal dynamics of atmospheric water inputs in tropical mountain forests of South Ecuador. *Hydrol Process* 25:344–352
- Román-Cuesta RM et al (2014) Synchronous fire activity in the tropical high Andes: an indication of regional climate forcing. *Glob Change Biol* 20:1929–1942
- Rossel F, Cadier E (2009) El Niño and prediction of anomalous monthly rainfalls in Ecuador. *Hydrol Process* 23:3253–3260
- Rossel F, Le Goulven P, Cadier E (1999) Repartition spatiale de l'influence de l'ENSO sur les précipitations annuelles en Equateur. *Revue des Sciences de l'Eau* 12:183–200
- Schubert SD, Suarez MJ, Pegion PJ, Koster RD, Bacmeister JT (2004) Causes of long-term drought in the U.S. Great Plains. *J Clim* 17:485–503
- Seager R, Kushnir Y, Herweijer C, Naik N, Velez J (2005) Modeling of tropical forcing of persistent droughts and pluvials over western North America: 1856–2000. *J Clim* 18:4065–4088
- Siegel S, Castellan NJ (1988) *Nonparametric statistics for the behavioral sciences*. Mc-Graw-Hill, Inc., New York
- Stillwell HD (1992) Natural hazards and disasters in Latin America. *Nat Hazards* 6:131–159
- Takahashi K, Montecinos A, Goubanova K, Dewitte B (2011) ENSO regimes: reinterpreting the canonical and Modoki El Niño. *Geophys Res Lett* 38:L10704. doi:10.1029/2011GL047364
- Taschetto AS, Gupta AS, Jourdain NC et al (2014) Cold tongue and warm pool ENSO Events in CMIP5: mean state and future projections. *J Clim* 27:2861–2885
- Tedeschi RG, Cavalcanti IFA, Grimm AM (2013) Influences of two types of ENSO on South American precipitation. *Int J Climatol* 33:1382–1400
- Trenberth KE, Smith L (2006) The vertical structure of temperature in the tropics: different flavors of El Niño. *J Clim* 19:4956–4973
- Trenberth KE, Stepaniak DP (2001) Indices of El Niño evolution. *J Clim* 14:1697–1701
- Venema V, Mestre O, Aguilar E et al (2012) Benchmarking monthly homogenization algorithms. *Clim Past* 8:89–115
- Vicente-Serrano SM, Beguería S, López-Moreno JI (2010a) A Multi-scalar drought index sensitive to global warming: the Standardized Precipitation Evapotranspiration Index–SPEI. *J Clim* 23:1696–1718
- Vicente-Serrano SM, Beguería S, López-Moreno JI, Angulo M, El Kenawy A (2010b) A new global 0.5° gridded dataset (1901–2006) of a multiscale drought index: comparison with current drought index datasets based on the Palmer Drought Severity Index. *J Hydrometeorol* 11:1033–1043
- Vicente-Serrano SM, López-Moreno JI, Gimeno L, Nieto R, Morán-Tejeda E, Lorenzo-Lacruz J, Beguería S, Azorin-Molina C (2011a) A multi-scalar global evaluation of the impact of ENSO on droughts. *J Geophys Res Atmos* 116:D20109. doi:10.1029/2011JD016039
- Vicente-Serrano SM, Beguería S, López-Moreno JI (2011b) Comment on “Characteristics and trends in various forms of the Palmer Drought Severity Index (PDSI) during 1900–2008” by A. Dai. *J Geophys Res Atmos* 116:D19112. doi:10.1029/2011JD016410
- Vicente-Serrano SM, Beguería S, Lorenzo-Lacruz J et al (2012) Performance of drought indices for ecological, agricultural and hydrological applications. *Earth Interact* 16:1–27
- Vicente-Serrano SM, Gouveia C, Camarero JJ et al (2013) The response of vegetation to drought time-scales across global land biomes. *Proc Natl Acad Sci USA* 110:52–57
- Vicente-Serrano SM, Van der Schrier G, Beguería S, Azorin-Molina C, Lopez-Moreno JI (2015) Contribution of precipitation and reference evapotranspiration to drought indices under different climates. *J Hydrol* 426:42–54
- von Storch H, Zwiers FW (1999) *Statistical analysis in climate research*. Cambridge University Press, Cambridge
- Vourlitis GL, de Souza Nogueira J, de Almeida Lobo F, Pinto OB Jr (2014) Variations in evapotranspiration and climate for an Amazonian semi-deciduous forest over seasonal, annual, and El Niño cycles. *Int J Biometeorol* 59:217–230
- Vuille M (1999) Atmospheric circulation over the Bolivian Altiplano during dry and wet periods and extreme phases of the southern oscillation. *Int J Climatol* 19:1579–1600
- Vuille M, Bradley RS, Keimig F (2000a) Climate variability in the Andes of Ecuador and its relation to tropical Pacific and Atlantic Sea Surface temperature anomalies. *J Clim* 13:2520–2535
- Vuille M, Bradley RS, Keimig F (2000b) Interannual climate variability in the Central Andes and its relation to tropical Pacific and Atlantic forcing. *J Geophys Res Atmos* 105(D10):12447–12460
- Vuille M, Bradley RS, Werner M, Keimig F (2003) 20th century climate change in the tropical Andes: observations and model results. *Clim Change* 59:75–99
- Vuille M, Francou B, Wagnon P et al (2008) Climate change and tropical Andean glaciers: past, present and future. *Earth Sci Rev* 89:79–96
- Wang Ch (2002) Atmospheric circulation cells associated with the El Niño–Southern Oscillation. *J Clim* 15:399–419
- Weng H, Behera SK, Yamagata T (2009) Anomalous winter climate conditions in the Pacific rim during recent El Niño Modoki and El Niño events. *Clim Dyn* 32:663–674
- Wilhite DA (1993) *Drought assessment, management and planning: theory and case studies*. Kluwer, Boston
- Xu H, Wang Y, Xie S-P (2004) Effects of the andes on eastern pacific climate: a regional atmospheric model study. *J Clim* 17:589–602
- Yeh S-W, Kug J-S, An S-I (2014) Recent progress on two types of El Niño: observations, dynamics, and future changes. *Asia-Pac J Atmos Sci* 50:69–81
- Yoon J-H, Yeh S-W, Kim Y-H, Kug J-S, Min H-S (2012) Understanding the responses of sea surface temperature to the two different types of El Niño in the western North Pacific. *Prog Oceanogr* 105:81–89
- Zhang T, Perlwitz J, Hoerling MP (2014) What is responsible for the strong observed asymmetry in teleconnections between El Niño and La Niña? *Geophys Res Lett* 41:1019–1025